

Indirect evidence that subsidence may be related to ground-water withdrawals includes water-level declines greater than 100 ft, subsurface collapse of well casings in the South Pleasant Valley subbasin and South Oxnard Plain subarea, required repeated leveling of irrigated fields for proper drainage, degraded operation of drainage ditches in agricultural areas, and lowering of levees along the Calleguas Creek in the South Pleasant Valley subbasin. In the Las Posas Valley and South Pleasant Valley subbasins, water-level declines of 50 to 100 ft have occurred in the upper-aquifer system, and declines of about 25 to 300 ft or more have occurred in the lower-aquifer system since the early 1900s (figs. 13 and 14). Owing to large water-level declines, the area of probable subsidence may be larger than that delineated by Ventura County and may include the Las Posas Valley subbasin and the remainder of the Pleasant Valley subbasin. By 1992, total subsidence in the Oxnard Plain subbasin could exceed the 2.6 ft measured during 1939–78 along the coastal traverse. Although the amount of subsidence from various sources remains unknown, ground-water withdrawals and oil and gas production probably are major causes of subsidence in the Oxnard Plain subbasin, and tectonic activity probably is a minor cause.

Water released by compaction of layers of fine-grained deposits within the upper- and lower-aquifer systems can be a significant additional one-time source of water to adjacent producing coarse-grained layers in the aquifer systems. Geochemistry data (Izbicki, 1996a, fig. 3) and geophysical data (EM and natural gamma logs in Appendix 5) indicate that fine-grained beds may be a significant source of the poor-quality water in areas such as the South Oxnard Plain subarea in the coastal region between the Hueneme and Mugu submarine canyons where saline fine-grained layers and seasonal pumpage may collectively contribute to poor-quality water.

SIMULATION OF GROUND-WATER FLOW

A numerical ground-water flow model of the two regional aquifer systems (upper aquifers and lower aquifers) in the Santa Clara–Calleguas Basin was developed to simulate steady-state predevelopment conditions prior to 1891 and transient conditions for the development period January 1891–December 1993. The model simulations provided information concerning predevelopment hydrologic conditions and aquifer response to changes in pumpage and recharge through time. Simulations were made using the three-dimensional finite-difference ground-water flow model (MODFLOW) developed by McDonald and Harbaugh (1988). Additional packages were incorporated into the ground-water flow model to simulate the routing of streamflow (Prudic, 1989), land subsidence (Leake and Prudic, 1991), and faults as horizontal barriers to ground-water flow (Hsieh and Freckleton, 1993).

Transient simulations were calibrated for the period of historical systematic data collection, which generally spans from the 1920s through 1993. The most important period of the calibration spans the period of reported pumpage (1984–93). Simulation results and model calibration provided insight into the conceptual model of the regional flow system, and into the limitations and potential future refinements of the regional-scale model. The model also was used to analyze the distribution of flow and changes in storage during 1984–93, to project future ground-water flow, and to evaluate alternatives to future projected ground-water flow. The analysis allowed assessment of water-resources management alternatives and of the effect that implementation of selected alternatives and geologic controls might have on recharge, coastal landward flow (seawater intrusion), land subsidence, ground-water movement, and overall resource management under climatically varying conditions that affect supply and demand.

Model Framework

The orientation, areal and temporal discretization, vertical layering, areal extent, and internal structural boundaries constitute the framework of the numerical ground-water flow model developed for this study. The model is an extension and refinement of the previously developed regional models and, as such, represents the RASA Program contribution to the continuing effort to evaluate and manage the ground- and surface-water resources of the Santa Clara–Calleguas Basin. Model attributes and related data have been added to the Geographic Information System (GIS) completed by the RASA Program (Predmore and others, 1997). The metadata that describe and document these additional GIS coverages are summarized in Appendix 1. The flow of information used to estimate and assemble the input data for the Recharge Package, Streamflow Package, and Well Package of the ground-water model is summarized in the flowcharts in Appendix 6.

Previous Models

Previous models of the area include basinwide digital Theissan-Weber Polygon superposition simulations of historical transient hydraulic and water-quality conditions for 1950–67 (California Department of Water Resources, 1974a,b, 1975), and numerical subregional ground-water flow models of the lower-aquifer system in the East and West Las Posas Valley subareas (CH2M HILL, 1993) and the upper- and lower-aquifer systems in the Santa Rosa Valley subarea (Johnson and Yoon, 1987). More recently, Reichard (1995) completed an extended and enhanced digital model based on the original Theissan-Weber Polygon model. Reichard extended this model areally to include the offshore coastal areas; like the regional model, it simulates the upper- and lower-aquifer systems in the Oxnard Plain subareas, the lower-aquifer system in the Las Posas Valley and Pleasant Valley subareas, and the upper-aquifer system in the Santa Clara River Valley subareas. The model uses estimates of recharge and pumpage for the historical simulation period (1984–89), which is the base period

used to evaluate the FGMA management goals. Reichard's model was used to simulate the flow of ground water and to generate response surfaces for use in an optimization model. In turn, the optimization model was used to test different ground-water and surface-water allocation schemes that would satisfy water demands and minimize coastal landward flow (seawater intrusion). Nishikawa (1997) completed a cross-sectional transport model of a vertical section through the Hueneme submarine canyon to test alternative conceptual models of seawater intrusion for predevelopment conditions and for 1929–93 developed conditions. A numerical wellbore hydraulic model of an aquifer test in the lower-aquifer system in the South Pleasant Valley subarea was completed to test alternative conceptual models of the vertical distribution of hydraulic properties (Hanson and Nishikawa, 1992, 1996).

Model Grid

The model grid is oriented at N. 27° W. and contains 60 rows and 100 columns discretized into square cells with sides 0.5 mi in length (figs. 7, 16, and A1.4). Average values of aquifer properties and initial hydraulic head are assigned to each cell; average initial hydraulic head for each cell is assigned at the center, or node, of each cell. The model contains two layers, one each for the upper- and lower-aquifer systems. The two model layers were made identical in areal extent everywhere in the landward part of the model domain (fig. 16). The top of the upper layer is aligned with the bottom of the fine-grained layers that separate the semiperched shallow aquifer from the upper-aquifer system throughout the Northwest and South Oxnard Plain subareas. The top of the upper layer is coincident with the land surface throughout the remainder of the upper layer. The bottom of the upper layer and the top of the lower layer are coincident with the bottom of the Mugu aquifer. This boundary generally occurs at a depth of 400 ft in the Oxnard Plain subareas. The bottom of the lower layer is coincident with the bottom of the Fox Canyon aquifer throughout most of the model area (figs. 7A and 8).

The model was extended offshore farther in the northwest corner of the lower layer than previous models (California Department of Water Resources, 1974a,b, 1975; Reichard, 1995). The areal extent of the layers was based on the outcrop areas on the geologic map (Weber and others, 1976) on land, and the seaward extent was based on bathymetry and submarine outcrops estimated from geology maps (Kennedy and others, 1987). The upper layer (upper-aquifer system) (fig. 16A) is an active flow region covering 374 mi², of which about 27 percent is offshore. The lower layer (lower-aquifer system) (fig. 16B) is an active flow region of 464.5 mi², of which about 41 percent is offshore.

Temporal Discretization

The model was used to simulate the period from January 1891 through December 1993. This 103-year historical simulation of ground-water and surface-water flow was temporally discretized into 3-month periods (stress periods) that represent the four seasons within a calendar year. For computational purposes, streamflow, recharge, and pumpage from wells are specified for each season of every year. Each season was discretized into 12 equal time steps to estimate flow and heads throughout the model.

Model Boundaries

The perimeter of the active flow region within the model represents the approximate limit of the ground-water flow system. The boundary is represented by a combination of no-flow, constant-flux, and general-head boundaries. Except where mountain-front recharge enters the model along the boundaries of the landward active flow region (fig. 17A), the landward model cells along this outer boundary of both model layers are represented as a no-flow boundary. No-flow boundaries occur where there is no flow of water between the active flow-region model cells and the adjacent areas. The bottom of the lower layer is also represented as a no-flow boundary; this layer generally is coincident with the base of the Fox Canyon aquifer except in the Santa Rosa Valley, East Las Posas, and parts of the Pleasant Valley subareas. These no-flow boundaries represent the contact with non-water-bearing rocks. Mountain-front recharge that enters along stream channels in the upper layer and at the outcrops of the Santa Barbara

Formation outside of the active flow system in the lower layer are constant-flux boundaries (described later in this section). The constant-flux boundaries are specified flows that change with every season (stress period) of each year for the period of simulation.

The offshore boundary in both layers is represented as a strong source-sink boundary; this boundary is located at the geographic location of the seawater intrusion front identified by Greene and others (1978). This boundary is represented in the model as a general-head boundary simulating inflow (source) of water from outside the model area or discharge (sink) of water from the boundary model cells to outside the model area. Flow at this boundary is proportional to the hydraulic-head difference between the equivalent freshwater head of the ocean along the submarine outcrops and the head of the model cells that are coincident with the boundary (fig. 16). Flow at this boundary is also proportional to the hydraulic conductance. Hydraulic conductance was determined during model calibration and represents the impediment to flow at the seawater intrusion boundary in each layer. For the purposes of this report, coastal inflow along this boundary is termed coastal landward flow (a surrogate for seawater intrusion) and outflow is termed coastal seaward flow.

The coastal flow of water through the submarine canyon outcrops is, in part, dependent on the equivalent freshwater head of seawater and the location of the freshwater/seawater interface. On the basis of EM and natural gamma logs (figure A5.1 in Appendix 5), the intrusion and movement of seawater occurs largely along the coarse-grained basal layers above regional unconformities. Chloride-concentration data, geophysical logs, and cross-section transport modeling of the Hueneme submarine canyon (Nishikawa, 1997) indicate that seawater intrusion is characterized by a relatively sharp front restricted to selected coarse-grained layers. Simulation of the seawater-interface boundary in this model assumed a position of the interface that is between the submarine outcrop and the coast. The interface location for the current model was inferred from the location estimated by Green and others (1978) for the lower-aquifer system (fig. 16B), transport model simulations (Nishikawa, 1997), and geochemical data from coastal monitoring wells (Izbicki, 1996a). The limitations of this assumption are further discussed in the "Model Uncertainty, Sensitivity, and Limitations" section.

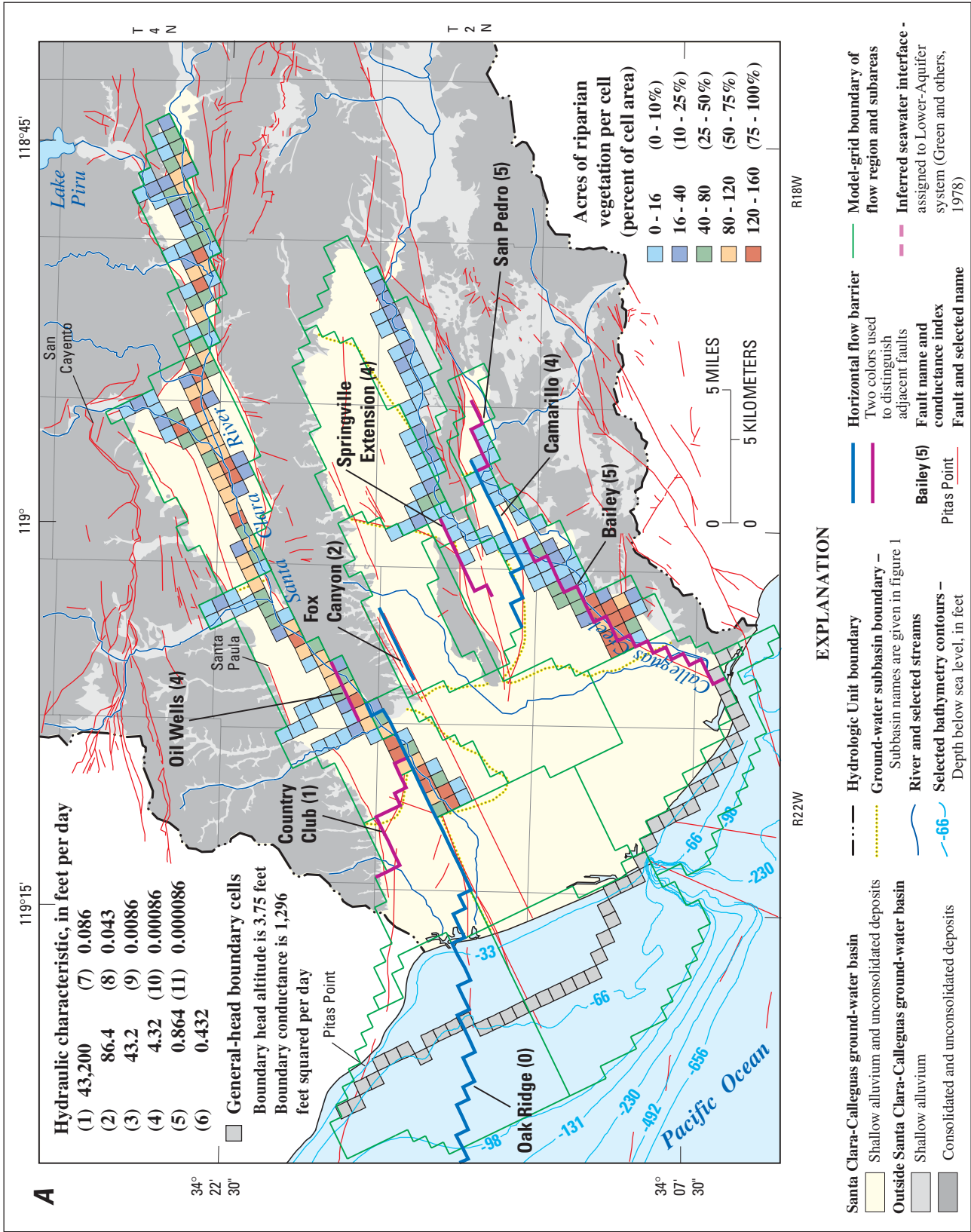


Figure 16. Location of model grid, location of general-head boundary cells with associated boundary head altitude and conductance, location of horizontal flow barriers and associated hydraulic characteristic, and location of evapotranspiration model cells and percent of riparian vegetation cover per cell in the Santa Clara-Calleguas ground-water basin, Ventura County, California. **A.** Upper-aquifer system. **B.** Lower-aquifer system.

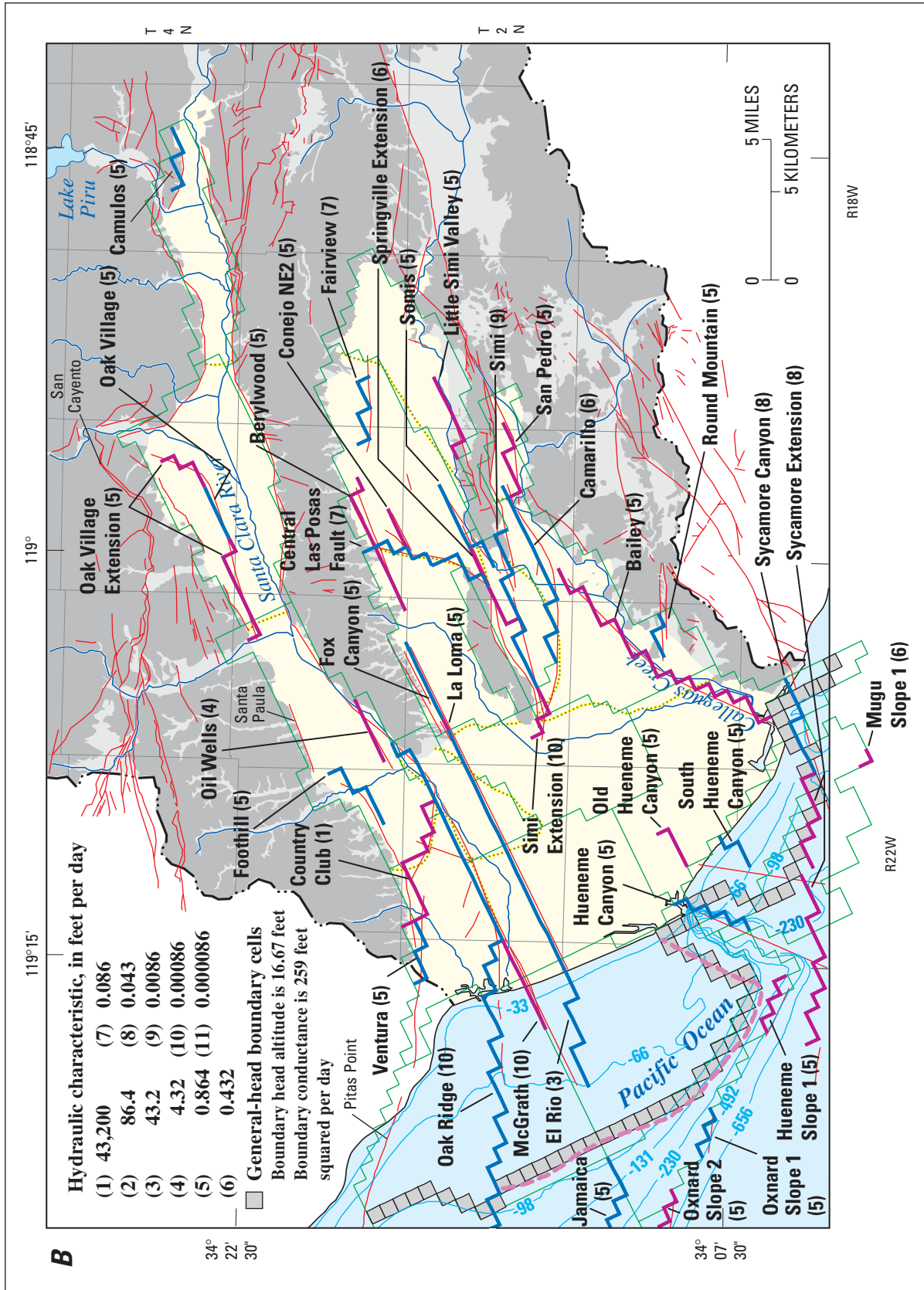


Figure 16—Continued.

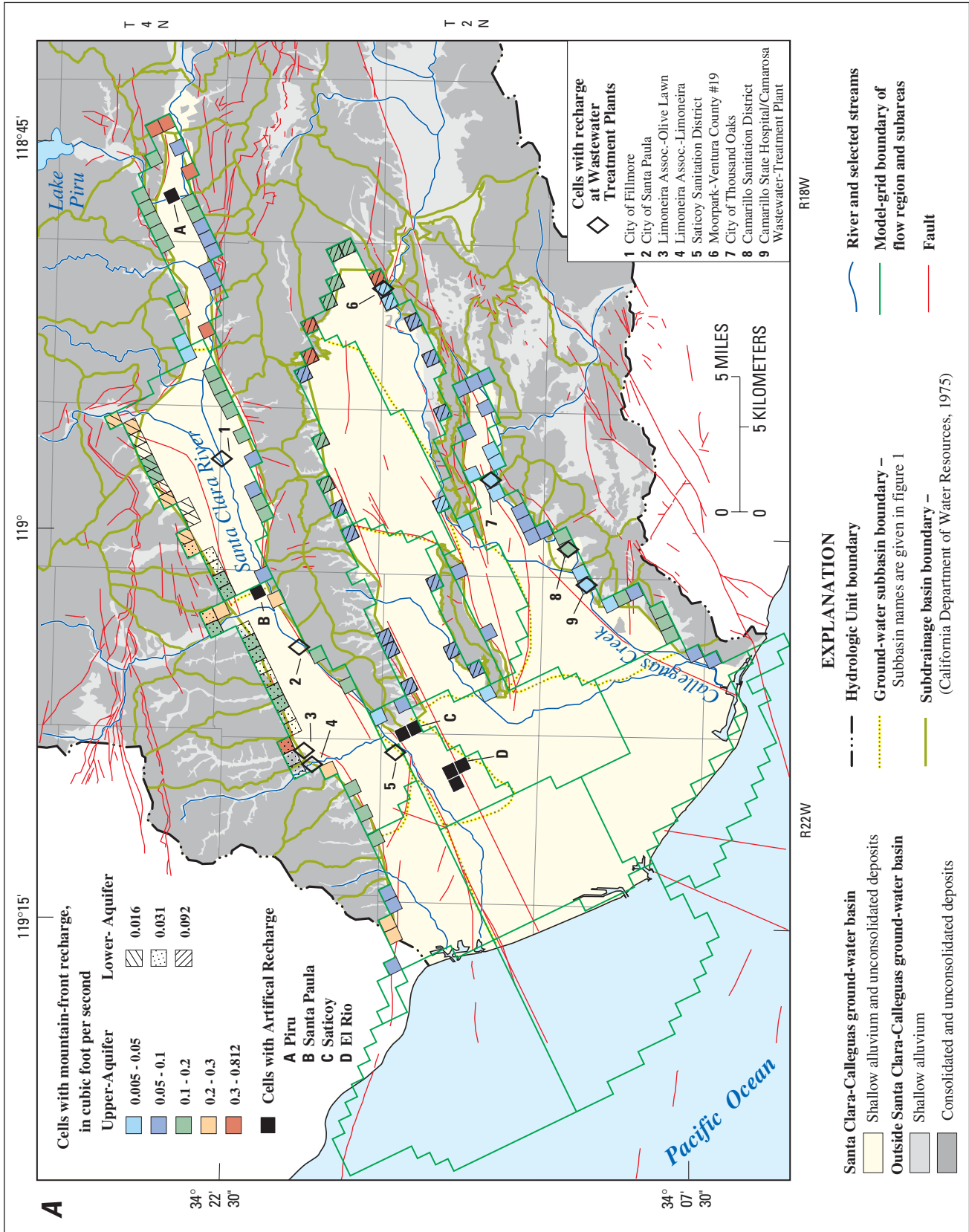


Figure 17. A Areal extent of model grid, location of model cells representing mountain-front, artificial, and treated wastewater recharge, and simulated rates of mountain-front recharge in the ground-water flow model of the Santa Clara-Calleguas ground-water basin, Ventura County, California.

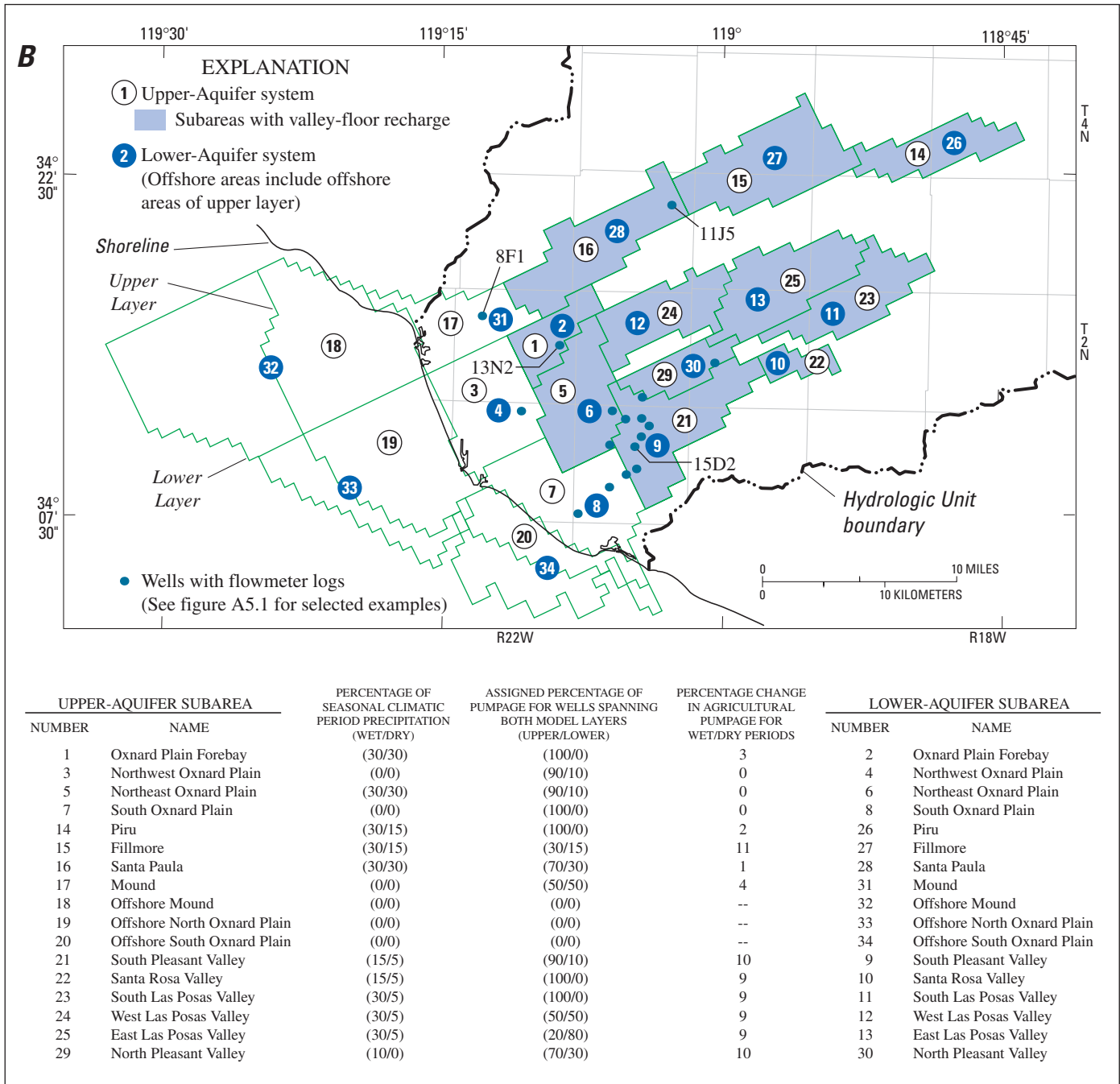


Figure 17—Continued. **B**, modeled subareas for the upper and lower aquifer systems, percentage of infiltration for seasonal precipitation during wet and dry climatic periods, location of wells with flowmeter logs, and the related percentage of pumpage assigned to wells spanning the upper and lower layers.

The offshore boundary representing the density-dependent seawater interface was simplified with a general-head boundary simulation which may limit the accuracy of the model for the simulation of some small-scale features in the coastal areas. Since the actual location of the boundary through time along the entire coast is unknown, the location of the boundary was held stationary at an average location for all simulations. A general-head boundary represents the inflow or outflow of water in a model cell and is represented by boundary head and conductance to flow between the model cell and the boundary. Flow between the boundary and the aquifer is controlled by the boundary conductance and by the head gradient, which is calculated by the model as the difference between the aquifer head in the model cell and the specified boundary head. The boundary head that represents the equivalent freshwater head of seawater at the depth of outcrop was estimated to be equivalent to 3.75 ft at 46 cells in the upper model layer (fig. 16A) and 16.67 ft at 65 cells in the lower model layer (fig. 16B). The equivalent freshwater head at the upper-aquifer boundary was estimated by dividing the depth to the submarine outcrop (150 ft below sea level) by 40 (density ratio between saltwater and freshwater); this outcrop was assumed to represent the basal coarse-grained layer in the Oxnard aquifer. In a similar manner, the equivalent freshwater head for the lower-aquifer boundary was estimated by dividing the depth to the submarine outcrop (667 ft below sea level) by 40; this outcrop was assumed to represent the basal coarse-grained layer in the Hueneme aquifer that generally occurs at a depth from 400 to 800 ft below land surface.

Boundary conductances initially were based on aquifer transmissivity and were modified during model calibration. An initial uniform conductance of 4,320 ft²/d was derived from the assumed values used in the extension of a model by Reichard (1995). The final distribution of conductances were 1,296 and 259 ft²/d for the upper- and lower-aquifer systems, respectively (fig. 16 A,B).

Faults are simulated as barriers to ground-water flow and as such provide peripheral and internal boundaries to the ground-water flow system. The peripheral faults, however, were not simulated as faults because they are coincident with no-flow boundaries.

The offshore Pitas Point and onshore Ventura, Foothill, Santa Paula, and San Cayento (thrust) Faults form the northern boundary of the ground-water flow system along the northern side of the Santa Clara River Valley subareas (fig. 16). The Oak Ridge Fault and South Mountain form the southern boundary of the ground-water flow system for the Mound (coastal) subarea and the inland subareas of the Santa Clara River Valley, respectively.

Internal faults are represented as a horizontal-flow barrier (Hsieh and Freckleton, 1993), across which the flow of water is proportional to a fault hydraulic characteristic determined during model calibration. The hydraulic characteristic is defined as the transmissivity of the fault divided by the fault width for confined aquifers. All faults in the lower-aquifer system and a subset of these faults in the upper-aquifer system were simulated as flow barriers (fig. 16). The most notable boundary occurs at the intersection of the Oak Ridge and Country Club (left-lateral reverse) Faults (fig. 16A) where the springs at Saticoy seeped ground water to the surface under predevelopment conditions. Ground-water level differences as great as 100 ft are reported across the Country Club Fault (Turner, 1975); data collected in the spring of 1992 suggest water-level differences of about 10 to 40 ft across this fault (Law/Crandall Inc., 1993).

Other faults at the subbasin boundaries acting as potential barriers to ground-water flow in the lower-aquifer system include a previously unmapped fault (hereinafter referred to the "Central Las Posas Fault"), which separates the lower-aquifer system between the West and East Las Posas Valley subbasins, and the extension of the Springville Fault, which separates the South Las Posas Valley and North Pleasant Valley subbasins (fig. 16B). The Camulos Fault, which forms the northeastern boundary of the Piru subbasin, also was included as a potential barrier to ground-water flow in the lower-aquifer system because of the extension of the ground-water model to the flanks of the mountain front. The Ventura Fault, which is aligned with the Pitas Point Fault (fig. 16) near the northwestern boundary in the Mound subbasin, also was included as a potential interior boundary to ground-water flow in the lower-aquifer system (fig. 16B).

Offshore faults of Pliocene to Miocene (?) age, mapped by Green and others (1978) and Kennedy and others (1987), were included as barriers to ground-water flow in the lower-aquifer system (fig. 16B). Some of these offshore faults (figs. 7, 9, and 16) are curvilinear and generally are subparallel to the submarine shelf; their northwest trend is typical of structures of the southern Coast Ranges Province. Other offshore faults trend west to southwest and are subparallel to the axes of the anticlines, synclines, and submarine canyons (figs. 7, 9, and 16) typical of structures of the Transverse Ranges Province. The northwest-trending faults included in the lower-aquifer system are an extension of the Sycamore Fault and minor fault traces, hereinafter referred to as “Hueneme slope 1,” “Mugu slope 1,” “Oxnard slope 1,” and “Oxnard slope 2” (fig. 16B). Offshore faults subparallel to the fold structures include extensions of the McGrath-Jamaica, Bailey, and El Rio Faults, and smaller faults coincident with the submarine canyons, hereinafter referred to as the “Hueneme Canyon,” “Old Hueneme Canyon,” and “South Hueneme Canyon” (fig. 16B).

Estimates of the hydraulic characteristics of faults were not available from aquifer tests or other field data. An initial uniform hydraulic characteristic of 0.09 ft/d was used to simulate faults as horizontal-flow barriers in the lower-aquifer system. The final distribution was derived by fitting simulated water-level changes near faults and water-level differences across faults to measured data; the distribution ranges from 43,200 to 8.6×10^{-5} ft/d (figs. 16A and B). On the basis of subsurface stratigraphy, mapping, and trenching (California Department of Water Resources, 1954; California State Water Resources Board, 1956; Weber and others, 1976; Jakes, 1979; Dahlen and others, 1990; Association of Engineering Geologists, 1991; Dahlen, 1992), selected faults were simulated to extend into the upper-aquifer system of the model for this study (fig. 16B). These faults include Oil Wells, Country Club, Camarillo, Fox Canyon, Springville Extension, Oak Ridge, San Pedro, and Bailey Faults.

Streamflow Routing and Ground-Water/Surface-Water Interactions

Streamflow was simulated using the streamflow-routing package developed by Prudic (1989). As the numerical model routes the streamflow from the inflow

locations through the stream network to the outflow locations, the model simulates streamflow infiltration to the ground-water flow system, ground-water discharge to the streams, streamflow diversions, and discharge of streamflow to the ocean. To simulate streamflow routing, each cell containing a reach of stream channel is assigned a segment number and a reach number within the segment. The network of streams and diversions contains 233 model cells (reaches) that are grouped into 30 segments (fig. 18A). The segments are groups of model cells that are coincident with the stream channels and represent the major parts of the river systems, which are divided at the points of confluence (fig. 18B). Streamflow entering the headwater segment of each stream and major tributary (fig. 18B) is specified for every season for the entire historical simulation period. The Santa Clara River and Calleguas Creek stream segments were linked at the confluence with their major tributaries and are shown in figure 18B. The altitude of the stage of the stream and streambed conductance for every reach of each segment and the altitudes of the top and base of the streambed are specified for each model cell.

For this study, streamflow infiltration was calculated using measured and estimated streamflow and the streamflow-routing program component of the ground-water flow model. Streamflow routing required construction of streamflow records for the major rivers and tributaries in the basin for January 1891 to the period of the continuous gaged streamflow record. Streamflow was estimated using regression equations with seasonal precipitation for wet and dry climatic periods (described later in Appendix 4, tables A4.1–A4.4). Precipitation data from three coastal, one intermontane, and two mountain precipitation stations were normalized and then used to produce “wet-day” nonlinear regression estimates of seasonal streamflow (Duell, 1992). Because precipitation data were available for coastal stations only for 1891–1905, an additional set of nonlinear relations was estimated for streamflow reconstruction for this early period of water-resources development. Correlations between precipitation and streamflow were better for the wettest periods (wet winters) than for the driest periods (dry summers). Most of the natural streamflow occurs during wet winters. Between 51 and 84 percent of the variance in natural streamflow during wet winters was estimated using the nonlinear relations between precipitation and gaged streamflow data.

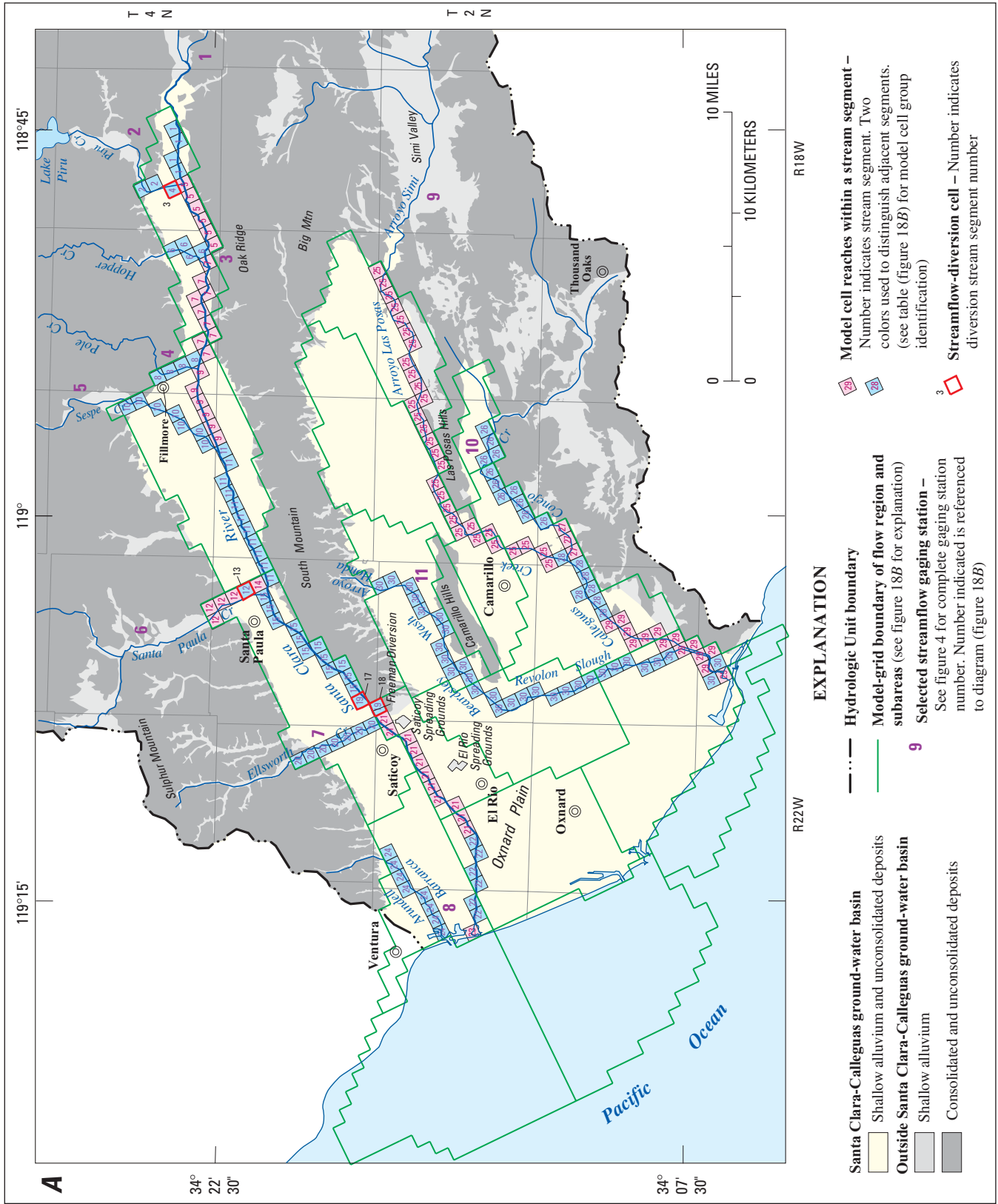


Figure 18 Streamflow network as simulated in the numerical model of the Santa Clara-Calleguas ground-water basin, Ventura County, California. **A**, Stream reaches and related gaging stations used for inflow and for calibrations of simulated streamflow. **B**, Schematic routing diagram of simulated streamflow network and streambed conductance for stream segments.

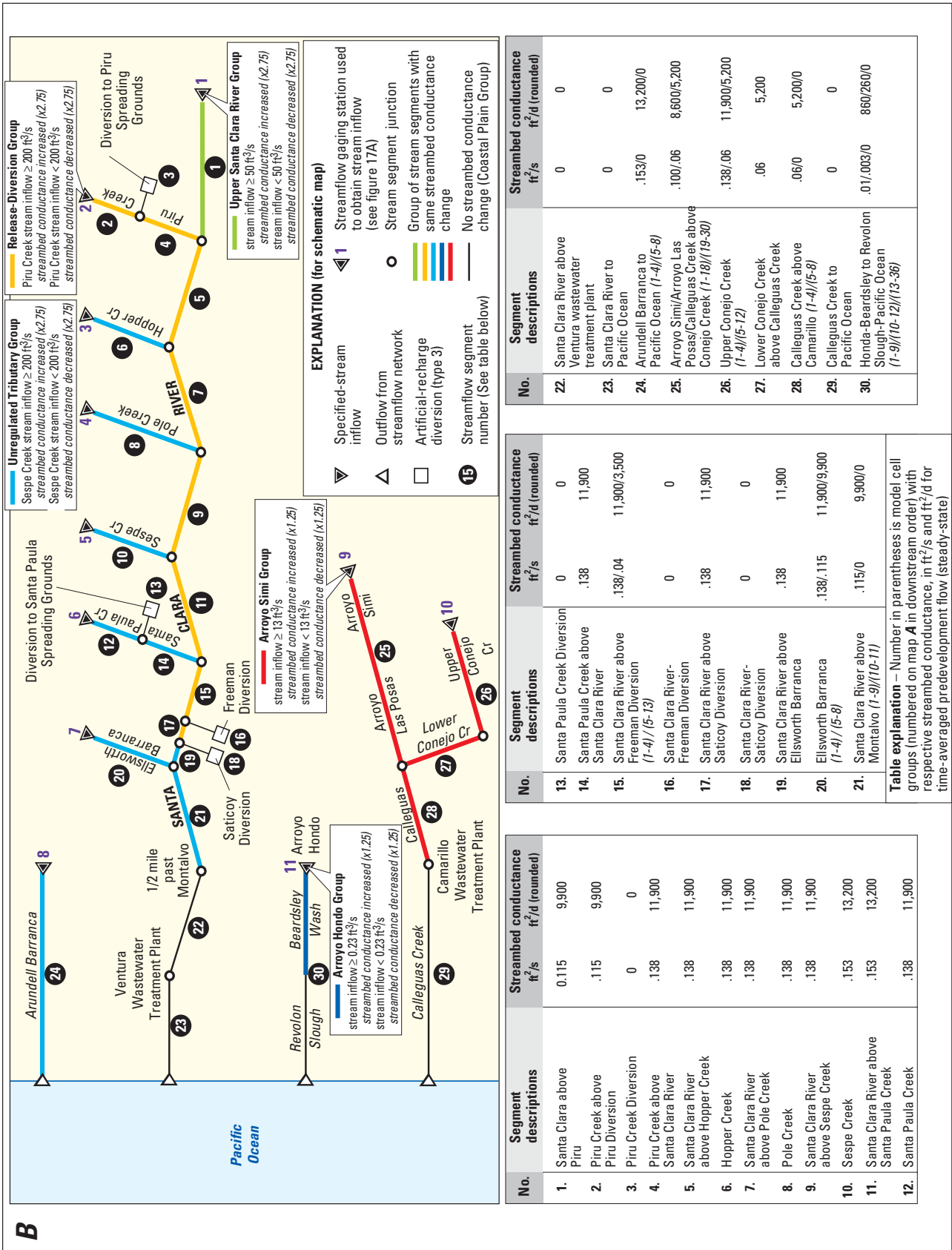


Figure 18—Continued.

The streamflow network represents gaged inflow along the Santa Clara River and tributaries, the Calleguas Creek and tributaries, Arroyo Hondo, and Arundell Barranca. Measured and estimated seasonal streamflow was used to simulate streamflow from 11 inflow points on the Santa Clara River, Piru Creek, Hopper Creek, Pole Creek, Sespe Creek, Santa Paula Creek, Ellsworth Barranca, Arrundell Barranca, Arroyo Hondo, Arroyo Simi, and Upper Conejo Creek (fig. 18B). Seasonal inflow rates were specified as the total seasonal flow volume divided by the number of days in the season for the period of record of each inflow site. For the period prior to historical records, nonlinear regressions of flow as a function of precipitation were used to estimate wet- and dry-period seasonal flows for the Santa Clara River, Piru, Hopper, Pole, Sespe, and Santa Paula Creeks and Arroyo Simi (Appendix 4, table A4.1–A4.4). Streamflow estimates for Ellsworth and Arrundell Barrancas, Arroyo Hondo, and Conejo Creek were based on seasonal ratios of gaged runoff to precipitation (modified rational method) for Pole and Hopper Creeks. The modified rational method was used for the period prior to the period for which streamflow-gaging data are available because there was no period of unregulated gaged streamflow that could be used to establish regression relations between streamflow and precipitation. Streamflow between the segments is the simulated streamflow routed from all upstream segments connected to a given segment. The simulation of predevelopment conditions used time-averaged streamflow estimates based on the geometric means and median streamflow values for the gaged streamflow (table 2) and the geometric-mean values of long-term runoff for ungaged tributaries.

The diversions at Piru, Santa Paula, and Saticoy and at the Freeman Diversion, which provide surface water for irrigation and artificial recharge, were simulated as losses from the stream network (fig. 18A,B). The streamflow-routing package of this model was altered to offer additional types of diversion (Appendix 2). The modified diversion type used for all four simulated diversions is referred to as an “artificial recharge diversion” [type 3 (Appendix 2)]; it will accept all streamflow available up to the specified amount of diversion. The seasonal amounts of

diversion were based on the UWCD’s reported total monthly diversions (Greg Middleton, United Water Conservation District, written commun., 1993).

Streamflow stages for all the reaches were estimated from relations between stream stage and streamflow at the inflow-gaging stations. The stream stage was held constant for all reaches in all segments for all simulations. Stream stage was initially estimated using extrapolated gaged height at the estimated predevelopment flow, which ranged from 0.3 to 4.5 ft for the steady-state flow rate at the inflow-gaging stations. However, stream stages were simplified and finally held to a constant value of 2.5 ft above the top of the streambed for all simulation periods and for all river reaches. The altitude of the top of the streambed was estimated from the arithmetic average of land-surface altitudes for the entire extent of the stream channel in each reach, which was estimated from digital altitude model data, 1:24,000-scale topographic maps, and gaging-station altitudes. The altitude of the base of the streambed was assumed to be 10 ft below the altitude of the top of the streambed for all the reaches for all time periods.

As water flows down the channels of the Santa Clara River and Calleguas Creek and their tributaries, some of the water infiltrates through the streambed and becomes ground-water recharge. In a few places, however, shallow ground water discharges to streams. In the model, this vertical flow between the stream and the aquifer is controlled by the streambed conductance and a vertical gradient that is driven by the difference between the specified stream stage and the simulated ground-water level. Stream stage for each stream reach was specified and was not changed for the entire simulation time. Streambed conductance initially was estimated as the product of the assumed channel width, channel length, and vertical hydraulic conductivity of the streambed deposits divided by the streambed thickness. Streambed conductance also can be estimated as the product of the streamflow and the fraction of streamflow loss divided by the streambed thickness. Although the actual stream channel width and streambed thickness vary spatially and with flow within many of the model cells, the streambed conductances were simplified into groups of segments with the same streambed conductance values (fig. 18B).

Initial estimates of streambed conductance were based on streamflow-loss estimates made in the early 1930s (California Department of Public Works, 1934) and in 1991 (Densmore and others, 1992); however, these direct estimates of streamflow losses vary widely—from 1 to 100 percent. Various mass-balance estimates for the Santa Clara River (Taylor and others, 1977; Dal Pozzo, 1992; Law/Crandall Inc., 1993) also have been made; these estimates also vary widely, ranging from 0 to 100 percent, with an average loss of about 22 percent. A water-balance approach yielded an estimate of streambed hydraulic conductivity of about 2 ft/d for the Santa Paula subarea (Law/Crandall Inc., 1993). The simulation of streamflow in the Santa Rosa Valley subarea model used vertical hydraulic conductivities of 3 ft/d for Arroyo Conejo and Conejo Creek and 1 ft/d for Arroyo Simi and an assumed streambed thickness of 1 ft (Johnson and Yoon, 1987). The assumed width is 50 ft, and the assumed streambed length was assumed to be the length of the cell (2,640 ft). Using values from Johnson and Yoon (1987), estimated streambed conductance is 13,200 ft²/d for Arroyo Simi and 39,600 ft²/d for Conejo Creek.

For the regional-scale model, the stream channel width initially was assumed to range from 50 to 200 ft, the length of the reach was assumed to be the length of the cell (2,640 ft), and the streambed thickness was assumed to be 10 ft. The streambed conductances were then put into six groups: the coastal plain group for which segments and reaches were set to a streambed

conductance of zero, the upper Santa Clara River group, the release-diversion group, the unregulated tributary group, the Arroyo Simi group, and the Arroyo Hondo group (fig. 18B). Streambed conductances for each group were increased and decreased from the predevelopment values and were changed on the basis of threshold values of stream inflows (fig. 18B). Results of model calibration indicate that the three groups of streambed conductances for the Santa Clara River system were increased when streamflows were greater than the flow threshold and decreased when they were less than the flow threshold by a factor of 2.75 with respect to conductances used to simulate time-averaged predevelopment conditions. The Arroyo Hondo and Arroyo Simi groups were increased when streamflows were greater than the flow threshold and decreased when streamflows were less than the flow threshold by a factor of 1.25 with respect to conductances used to simulate time-averaged predevelopment conditions. This change in conductance is believed to reflect the change in channel width and is similar to the factors of 1.2 to 2.0 used for the simulation of the streamflow routing of the Little Humboldt River, Nevada (Prudic and Herman, 1996). The final distribution of streambed conductances ranges from 0 to 13,200 ft²/d (fig. 18B) for time-averaged predevelopment conditions. These final values are the product of model calibration for time-averaged predevelopment (steady-state) conditions and of comparisons of the streamflow hydrographs for historical downstream streamflow and diversions.

Mountain-Front Recharge

Natural recharge along the model boundaries, mountain-front recharge, was simulated as a constant-flux inflow for each season (fig. 17A,B). Mountain-front recharge was simulated as a seasonally varying estimate of runoff specified as infiltration at the mountain front for 64 ungaged surface-water subdrainage basins (California Department of Water Resources, 1975, plate 2) that surround and drain into the 12 ground-water subbasins of the Santa Clara–Calleguas Basin (figs. 1 and 17A). The average for total wet- and dry-seasonal precipitation was estimated for each ungaged subdrainage basin. The modified rational method was used to estimate the seasonal runoff for each of the 412 seasons in the simulated historical period January 1891–December 1993. The ratio of runoff from Pole or Hopper Creeks to the total seasonal precipitation for these two index subdrainage basins ranged from 0 to 7, but most of the ratios were less than 0.25. These ratios were comparable to the fraction of precipitation as ground-water recharge estimated from detailed water-balance studies completed by Blaney (California Department of Public Works, 1934) for water years 1928–32. Blaney estimated annual fractions of rainfall penetration ranging from 0.01 to 0.17 for dry years and from 0.06 to 0.34 for wet years. Using the modified rational method, estimated ratios greater than 1 would result in a runoff total that is greater than the average precipitation. On the basis of previous infiltration studies in the Santa Clara–Calleguas Basin (California Department of Public Works, 1934; Taylor and others, 1977; Densmore and others, 1992), most fractions of runoff that infiltrate are less than 0.9. The ratios selected for estimating recharge were from Pole Creek for winter and fall seasons and from Hopper Creek for spring and summer seasons. When any ratio exceeded 0.9, the ratio from the other index subarea was used. When both ratios exceeded 0.9, the ratios were replaced with the geometric mean of ratios less than or equal to 0.9 for that respective wet or dry climatic season. The estimated mountain-front recharge for each subdrainage basin was then equally distributed to one or more cells that are coincident with the stream channels at the model boundary (fig. 17A). The resulting recharge estimates for an individual cell was reduced to 3.4 ft³/s if the estimated recharge value

exceeded that amount. This value was determined from streamflow seepage measurements of low flows on Santa Paula Creek (Dal Pozo, 1992).

The estimated total time-averaged mountain-front recharge rate used for the steady-state simulation of predevelopment conditions was 12,500 acre-ft/yr. The constant rate of recharge for the steady-state simulation, which was based on the geometric-mean ratios, was used to estimate the time-averaged runoff from each mountain-front subdrainage basin. The estimated total time-varying mountain-front recharge rate used for transient-state simulation of historical conditions ranged from 6,000 acre-ft/yr in 1923 to 80,600 acre-ft/yr in 1993. Mountain-front recharge was simulated as injection wells, with a constant rate of recharge per season, for 119 model cells in the uppermost active layer that coincide with the stream channels in the ungaged-tributary drainage basins (fig. 17A).

Additional recharge as direct infiltration on the outcrops of the San Pedro Formation (fig. 7A) was estimated based on wet-period average winter precipitation for 54 model cells that coincide with the San Pedro Formation in the Fillmore, Santa Paula, and Las Posas Valley subareas (figs. 7A and 17A). The recharge rate representing deep infiltration over the outcrops was estimated using the modified equation developed by the Santa Barbara County Water Agency (1977):

$$\text{Recharge} = (P_{\text{wet}} - 17 \text{ inches})/1.55,$$

where

Recharge is average recharge rate, in inches per year, and P_{wet} is wet-period total annual precipitation of 20.75 in. for outcrops surrounding the Las Posas Valley subareas and 21.25 in. for outcrops on the north side of the Santa Clara River Valley subareas.

This method assumes uniform temporal and areal distributions of rainfall without regard to the intensity of individual storms. The resulting recharge rate is reduced by the fraction of wet years (32 years) in the total period of historical simulation (103 years). The resulting estimates for a constant average recharge were 470 acre-ft/yr for East Las Posas Valley subarea, 740 acre-ft/yr for South Las Posas Valley subarea, 400 acre-ft/yr for West Las Posas Valley subarea, 240 acre-ft/yr for Fillmore subarea, and 320 acre-ft/yr for Santa Paula subarea. Thus, the long-term average recharge to the lower-aquifer system for a total bedrock recharge was about 2,200 acre-ft/yr (table 4).

Valley-Floor Recharge

Direct infiltration of precipitation on the valley floors, hereinafter referred to as “valley-floor recharge,” was simulated using the model recharge package and was distributed equally to all cells in each valley floor of the Piru, Fillmore, Santa Paula, Las Posas Valley (East, West, and South), Pleasant Valley (North and South), Oxnard Plain Forebay, and Santa Rosa Valley, and the Northeast Oxnard Plain subareas ([fig. 17B](#)). The estimated total time-averaged recharge rate used for the steady-state simulation of predevelopment conditions was 4,800 acre-ft/yr, which is based on the geometric-mean ratios of runoff to precipitation at Pole and Hopper Creeks. The total time-varying valley-floor recharge used for the transient-state simulation of historical conditions was varied seasonally using the same percentages of infiltration of irrigation based on model calibration ([fig. 17B](#)). The recharge rates ranged from 18,300 acre-ft/yr for dry-year periods to 32,700 acre-ft/yr for wet-year periods ([table 4](#)).

Artificial Recharge

Recharge of infiltration of diverted streamflow, discharge of treated sewage effluent, and irrigation return flow were simulated as a constant-flux inflow using the MODFLOW well package. No artificial recharge was applied to predevelopment (steady-state) conditions. For developed (transient-state) conditions, infiltration of diverted streamflow was applied for the period 1928–93, infiltration of irrigation was applied for the period 1891–1993, and infiltration of treated sewage effluent was applied for the period 1936–93.

Recharge of diverted streamflow was simulated at the artificial-recharge spreading grounds (basins) operated by the UWCD in the Piru and Santa Paula subareas and in the Oxnard Plain Forebay subarea ([figs. 4 and 18A](#)). The quantity of artificial recharge simulated in the model ([fig. 11A](#)) was based on reported annual and seasonal amounts of recharge

(United Water Conservation District, 1986, plate 5a,b; Greg Middleton, United Water Conservation District, written commun., 1993).

Recharge of treated sewage effluent was simulated as constant-flux inflows using the MODFLOW well package. This recharge was based on reported and extrapolated annual amounts of treated sewage discharge (California Department of Water Resources, 1975; W.D. Jesena, California Regional Water Quality Control Board, written commun., 1991; E.G. Reichard, U.S. Geological Survey, written commun., 1993; Mitri Muna, Ventura County Waterworks, written commun., 1995) and was assigned to nine model cells ([fig. 17A](#)) at a rate reduced to 74 percent (Farnsworth and others, 1982) of the reported or interpolated annual rate of discharge to account for the free-water surface evaporation while in percolation ponds and streambeds. The treated sewage effluent represents discharge from the city of Fillmore during 1958–93, the city of Santa Paula during 1937–93, the Limoneira Association at Olive Lawn Farm and Limoneira Farm during 1975–93, the Saticoy Sanitation District during 1960–93, the Camarillo Sanitation District during 1959–93, the city of Thousand Oaks during 1962–72, the Camarillo State Hospital during 1960–80, the Camarosa wastewater-treatment plant during 1981–93, and the Moorpark-Ventura County wastewater-treatment plant No. 19 during 1973–93. Additional sewage effluent discharged from the city of Thousand Oaks Hill Canyon Plant is represented as streamflow during 1973–93. Treated sewage effluent from the percolation ponds near the Santa Clara River which was used by the city of Piru during 1975–93 was not included because of the small volumes of discharge (Charles Rogers, city of Piru, oral commun., 1995). Total treated-sewage effluent that becomes ground-water recharge was applied at a constant rate for all four seasons of every year; the rate increased from 20 acre-ft/yr in 1936 to 9,000 acre-ft/yr in 1993 ([fig. 11A](#)).

Irrigation return flow was estimated as a percentage of the total applied water and included ground-water and surface-water components for many of the subareas. This recharge was simulated as a constant-flux inflow using the MODFLOW well package for the uppermost layer of the model. Irrigation return flow was estimated for each of the land-use periods and held constant for the same periods used to estimate ground-water pumpage (fig. 11A,B). The irrigation return flow was applied over a 245-day growing period prior to 1927 and applied uniformly for the entire year for the remainder of the simulation period. It was applied over the entire year because infiltration through the unsaturated zone tends to extend the period of infiltration. The 1969 land-use map was used to estimate the distribution of irrigation return flow for the period of reported pumpage, 1973–93. The assumed infiltration ranged from 5 to 30 percent of applied irrigation water for all subareas and was varied for wet- and dry-year periods (fig. 17B). The percentage of irrigation return flow was estimated during model calibration. Irrigation return flow ranged from less than a few hundred acre-feet per season for the Mound and North Peasant Valley subareas to about 1,400 acre-ft per season for the Santa Paula subarea (fig. 11). Total irrigation return flow ranged from 14,600 acre-ft/yr for the 1890s to 51,500 acre-ft/yr for the drought period 1987–91.

Other Sources of Recharge

Other sources of recharge include flow of water along some fault zones from older (Miocene age) marine sedimentary rocks and brines related to oil deposits. Some of these potential sources of water may yield water of poor quality or water of different chemical composition. Water-chemistry data indicate that the amount of leakage from the deeper, older formations in the South Oxnard Plain subarea and the South Pleasant Valley subarea probably is small (Izbicki, 1991, 1996a); therefore, it was not included in the current regional simulations.

Another source of potential recharge is leakage of the semiperched water to the upper-aquifer system. Leakage of semiperched ground water may enter the

upper- and lower-aquifer systems through failed and abandoned wells. Because the initial water-chemistry data indicate a potentially small effect and because water-level hydrographs indicate a potentially complicated relation, this element was not included in the current regional simulation. Any potential leakage through intraborehole flow or failed wells was included collectively and simulated in the irrigation-return-flow component.

Natural Discharge

Natural discharge is simulated as seaward coastal flow through submarine outcrops and as evapotranspiration (ET) along the flood plains of the Santa Clara River and Calleguas Creek. The coastal flow of water to the ocean was determined through model simulation and calibration; it is described in the “Model Boundaries” section.

ET by riparian vegetation (phreatophytes) and evaporation from bare soil were simulated at 306 model cells of layer 1 (upper-aquifer system) (fig. 16A) using the MODFLOW evapotranspiration package. Using previous estimates (California Department of Public Works, 1934), a maximum ET rate of 2.4 ft/yr was assumed when the water table is at land surface, and ET was assumed to decrease linearly to zero when the water table reaches a depth of 10 ft or more below land surface. The ET rate was multiplied by the ratio of riparian vegetation area to total model-cell area to account for the riparian vegetation density in each model cell. The weighting factor is the number of acres of riparian vegetation, estimated from the 1912, 1927, 1932, and 1950 land-use maps, for each cell divided by the total number of acres (160) in a model cell. The composite ET rates and the model cells with the potential for ET in 1912, 1927, 1932, and 1950 (Conejo Creek area) were used for the predevelopment and historical simulation for 1891–1926. The ET surface remained the same for the remainder of the simulation periods, but the ET rates were updated to reflect changing ET acreage. Thus, acreage for riparian vegetation was updated using the 1932 acreage for 1927–46 and the 1950 acreage for the remainder of the simulation period.

Pumpage

The simulation of ground-water withdrawal from wells as pumpage required a compilation of historical estimates that include indirect estimates of agricultural pumpage based on land use (1891–1977), reported municipal pumpage (1914–77), and metered agricultural and municipal pumpage (1978–93) reported to and compiled by the UWCD and the FGMA. Estimated pumpage ranged from 34,800 acre-ft for the drought years of the 1920s to a maximum pumpage of 301,400 acre-ft for the 1990 drought year. Estimated pumpage is shown in [figure 11B](#) for the period of simulation. The annual and biannual pumpage estimates were temporally distributed for model input to the seasonal intervals on a well-by-well basis. The initial vertical distribution of pumpage between aquifer systems was based on well construction (Predmore and others, 1997) and wellbore flowmeter studies completed as part of the RASA studies ([table 5](#)). For wells completed only in the upper-aquifer system, all water was derived from the upper model layer, and for wells completed only in the lower-aquifer system, all water was derived from the lower model layer. For wells that were completed in both the upper- and lower-aquifer systems, a percentage of total well pumpage was assigned to the upper and lower layers on the basis of wellbore flowmeter data, slug tests, and model calibration ([fig. 17B](#)). Pumpage from wells with no construction data was distributed using these same assumed percentages of pumpage. The distribution of pumpage from the upper- and lower-aquifer systems, estimated from the land-use map for agricultural pumpage, also used these same percentages for all the subareas.

Indirect estimates of agricultural pumpage were compiled for five land-use periods that span from 1912 to 1977 (Koczot, 1996). The compilation was based on land-use maps for 1912, 1932, 1950, and 1969 and on a mosaic of areal photos from 1927 (Predmore and others, 1997). The distribution of estimated agricultural pumpage was based on well locations reported in 1987 and on percentages of pumpage within each subarea. The estimates of agricultural pumpage were distributed over time on the basis of major changes in crop types and climatic periods. Because the growing periods of the various crop types spanned an 8-month period, pumpage was estimated and distributed using a 245-day growing season (Koczot, 1996) spanning March through October for the period 1912–26. The growing season was extended to 275 days, spanning from March through November for the period 1927–77. The extension of the growing period was based on inspection of water-level hydrographs and the wider variety of truck and orchard crops introduced during this period. The magnitude of pumpage was reduced during wet climatic periods and increased during dry climatic periods. The percentage change in agricultural pumpage was based on the ratios of wet-year to average-annual reported pumpage for each subarea and dry-year to average-annual reported pumpage ([fig. 17B](#)). The reported municipal pumpage for the cities of Ventura, Camarillo, and Oxnard and the Channel Island Community Services District; pumpage for the fish hatchery in the southern end of the Piru subarea; and pumpage of artificial recharge in the Oxnard Plain Forebay were estimated independently and combined with agricultural pumpage for input to the ground-water flow model for the period of simulation prior to 1983 ([fig. 11B](#)).

Regional management of ground-water resources was implemented by the State of California in 1983 with the creation of the Fox Canyon Groundwater Management Agency (FGMA) for controlling seawater intrusion. The FGMA jurisdiction covers part of the Santa Clara–Calleguas Basin and includes the Oxnard Plain, Oxnard Plain Forebay, Pleasant Valley, and Las Posas Valley subareas ([figure 26](#) presented later in the section “Analysis of Ground-Water Flow”). Reported pumpage was compiled from the technical files of the FGMA and the UWCD for the period July 1979–December 1993. These data generally consist of semiannual totals of user-reported agricultural, nonagricultural (municipal, industrial, and domestic), and total pumpage. Agricultural pumpage was distributed based on a 275-day growing period and the nonagricultural pumpage was distributed equally over seasonal periods of the flow model. Pumpage for 1980, which was based on water-level hydrographs and on climate data, was used for the period 1978 through 1980. When only total pumpage was reported, that pumpage was assumed to be for agricultural use. Early pumpage data were incomplete for the Las Posas Valley, the eastern part of the Pleasant Valley, and the Santa Rosa Valley subareas. For these areas, 1984 FGMA-reported pumpage was used to represent pumpage for 1978 through 1983. Total reported annual pumpage ranged from as little as 850 acre-ft in the South Las Posas Valley subarea during 1992 to as much as 107,300 acre-ft in the Oxnard Plain and Oxnard Plain Forebay subareas during 1990.

Hydraulic Properties

Estimates of transmissivities and storage coefficients for both model layers and estimates of coefficients of vertical leakance between layers are required to simulate the flow of ground water. Estimates of the horizontal conductance of faults are required to simulate potential barriers to ground-water flow, and the vertical conductance of streambeds is required to simulate the flow of water between shallow ground water and streamflow. The average values for

these parameters are used in the model and represent the hydraulic properties which are the spatial averages over individual model cells. They generally are held constant through time. Except for fault hydraulic characteristics, vertical conductances of the streambed, subsidence parameters, and areas where model layers were extended, the initial estimates for all the model parameters were derived largely from the spatial estimates used in previous ground-water flow models of the basin (California Department of Water Resources, 1974a,b, 1975; Johnson and Yoon, 1987; CH2M HILL, 1993; Reichard, 1995).

Transmissivity

Transmissivity is the product of the hydraulic conductivity and saturated thickness of the aquifers; therefore, transmissivity values may be affected by changes in saturated thickness. Transmissivity throughout much of the modeled area is associated with the basal coarse-grained layers of the aquifers that remain saturated; many parts of the aquifers are confined or show water-level changes that are a relatively small percentage of the saturated thickness. Because the effective saturated thickness is relatively constant over most of the model area, this model uses constant transmissivities for the entire period of simulation. Transmissivities estimated from specific-capacity tests were used to simulate ground-water flow using the Theissan-Weber Polygon model (California Department of Water Resources, 1975). Estimates for the upper-aquifer system range from 650 ft²/d along the northern edge of the Santa Paula subarea to more than 53,000 ft²/d in the northern Oxnard Plain and 67,000 ft²/d north of the Mugu submarine canyon (California Department of Water Resources, 1975, pl. 8). Estimates for the lower-aquifer system range from about 1,300 ft²/d near Moorpark to 53,000 ft²/d north of Port Hueneme (California Department of Water Resources, 1975, pl. 8). The coastal estimates from the Theissan-Weber Polygon model were extended as constant values to the adjacent offshore regions by Reichard (1995, fig. 10).

The current model modified these estimated transmissivities and used additional estimates beyond the areal extent of the previous models for the upper-aquifer system (layer 1) in the Las Posas Valley, Pleasant Valley, and Santa Rosa Valley subareas and for the lower layer in the Santa Clara River Valley subareas (fig. 17B and 19A). The estimated transmissivities for the upper-aquifer system (layer 1) ranged from 1.3 ft²/d for the Las Posas Valley subarea to about 73,800 ft²/d for the Oxnard Plain Forebay (fig. 19A); the estimated transmissivities for the lower-aquifer system (layer 2) ranged from about 38 to 26,500 ft²/d. A constant transmissivity of about 4,700 ft²/d was assigned to the lower-aquifer system (layer 2) for the offshore part of the Mound subarea on the basis of the estimated thicknesses and the hydraulic conductivities used onshore (fig. 19A).

The final estimates of transmissivities in the calibrated model for both model layers were refined for each subarea using the sum of transmissivities for the aggregate thicknesses of the coarse-grained and fine-grained deposits in each model cell (fig. 20). The transmissivity of the coarse-grained deposits was determined as the product of the thickness of the coarse-grained deposits (estimated from resistivity logs) and a geometric-mean hydraulic conductivity (estimated from slug tests). The transmissivity of the fine-grained deposits is the product of the thickness of fine-grained deposits and an assumed hydraulic conductivity of 0.1 ft/d.

Some of the transmissivities from previous regional models for the upper-aquifer system were reestimated using estimates of a geometric-mean hydraulic conductivity from the slug tests and the aggregate thicknesses of the coarse- and fine-grained deposits (fig. 20A). Transmissivity estimates were made using a hydraulic conductivity of 35.1 ft/d for the coarse-grained deposits in the Piru and Santa Paula subareas; these values were based on slug-test values that range from 18 to 88 ft/d in monitoring wells completed in these subareas (E.G. Reichard, U.S. Geological Survey, written commun., 1995).

Transmissivities for the upper-aquifer systems (layer 1) of the Las Posas Valley, Santa Rosa Valley, and Pleasant Valley subareas were needed to extend the

upper model layer of the previous models for all the subareas (figs. 17B and 19A). The transmissivities of the coarse-grained deposits of the East Las Posas Valley subarea were estimated using a geometric-mean hydraulic conductivity of 0.3 ft/d, which was based on slug-test values that range from 0.21 to 0.47 ft/d in monitoring wells completed in this subarea.

Transmissivities of the coarse-grained deposits of the West Las Posas Valley subarea were estimated using a geometric-mean hydraulic conductivity of 0.19 ft/d, which was based on slug-test values that range from 0.14 to 0.27 ft/d in monitoring wells completed near Arroyo Hondo. Transmissivities of the coarse-grained deposits of the South Las Posas Valley subarea were estimated using a geometric-mean hydraulic conductivity of 1.58 ft/d, which was based on slug-test values that range from 0.48 to 3.49 ft/d in monitoring wells completed in the subarea. The transmissivities of the coarse-grained deposits of the Santa Rosa Valley subarea (fig. 20) were based on two sets of hydraulic conductivities: A reported value of 80 ft/d for the Saugus Formation (Johnson and Yoon, 1987) was used to represent the upper and lower aquifers on the west side of the San Pedro Fault; reported values of 150 and 120 ft/d for the alluvium and the Santa Margarita Formation, respectively, were used for the east side of the San Pedro Fault (Johnson and Yoon, 1987). Transmissivity for the Pleasant Valley subarea was estimated using a geometric-mean hydraulic conductivity of 8.8 ft/d for the coarse-grained deposits, which is based on slug-test values that range from 0.13 to 11.8 ft/d in monitoring wells in this subarea.

Estimates of hydraulic conductivities for the lower-aquifer system (layer 2) deposits range from 1 to 8 ft/d for monitoring wells completed in the northern part of the Oxnard Plain subarea and from 5.5 to 44 ft/d for monitoring wells completed in the Piru and Santa Paula subbasins (E.G. Reichard, U.S. Geological Survey, written commun., 1992). Transmissivities for the coarse-grained deposits within layer 2 of the Santa Clara River Valley subareas were estimated using a geometric-mean hydraulic conductivity of 15.4 ft/d.

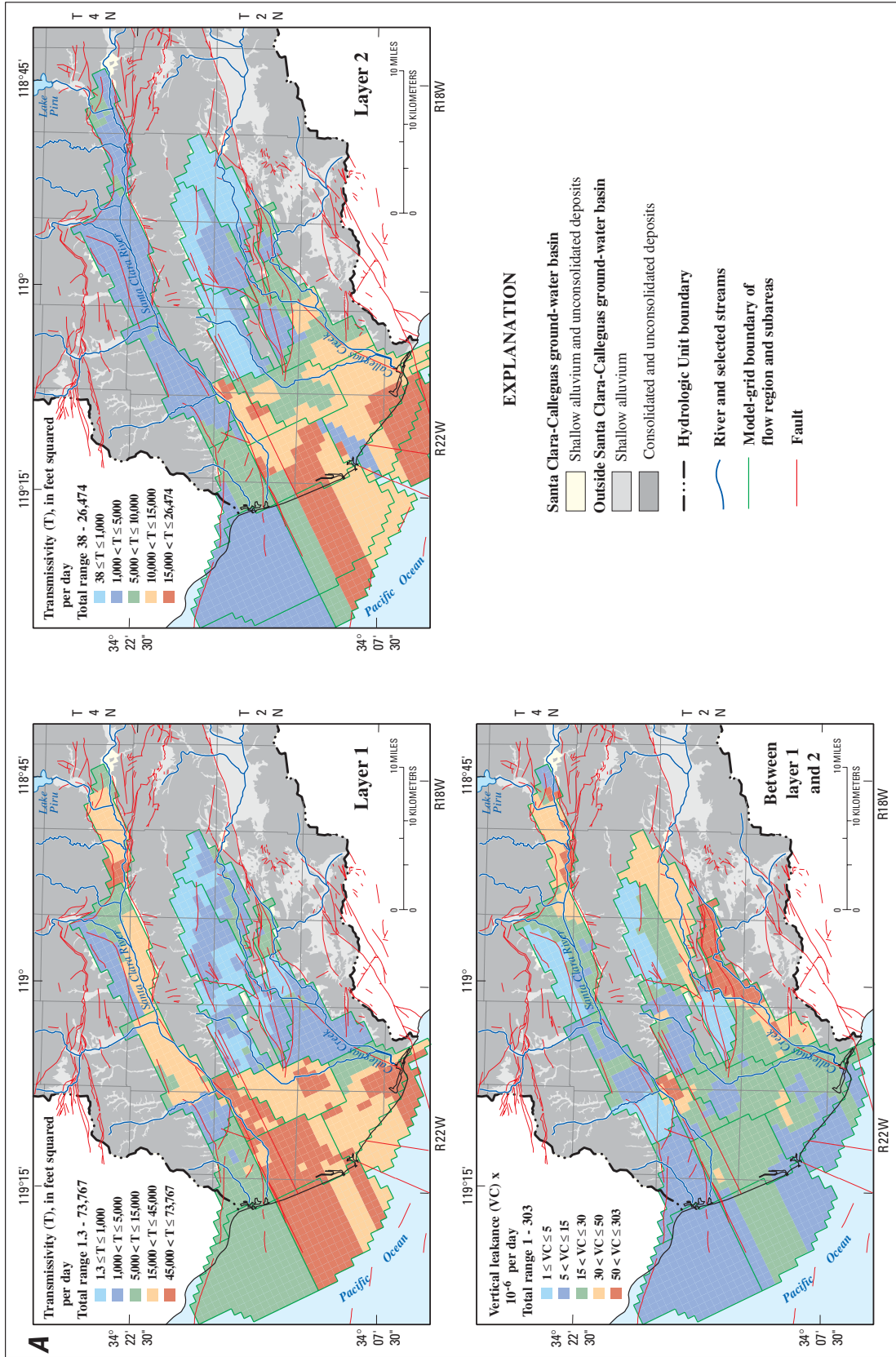


Figure 19. Distribution of hydraulic properties in layers 1 and 2 of the model of the Santa Clara–Calleguas ground-water basin, Ventura County, California. **A.** Distribution of transmissivity in model layers 1 and 2, and vertical leakage between model layers 1 and 2. **B.** Storage coefficient for model layers 1 and 2.

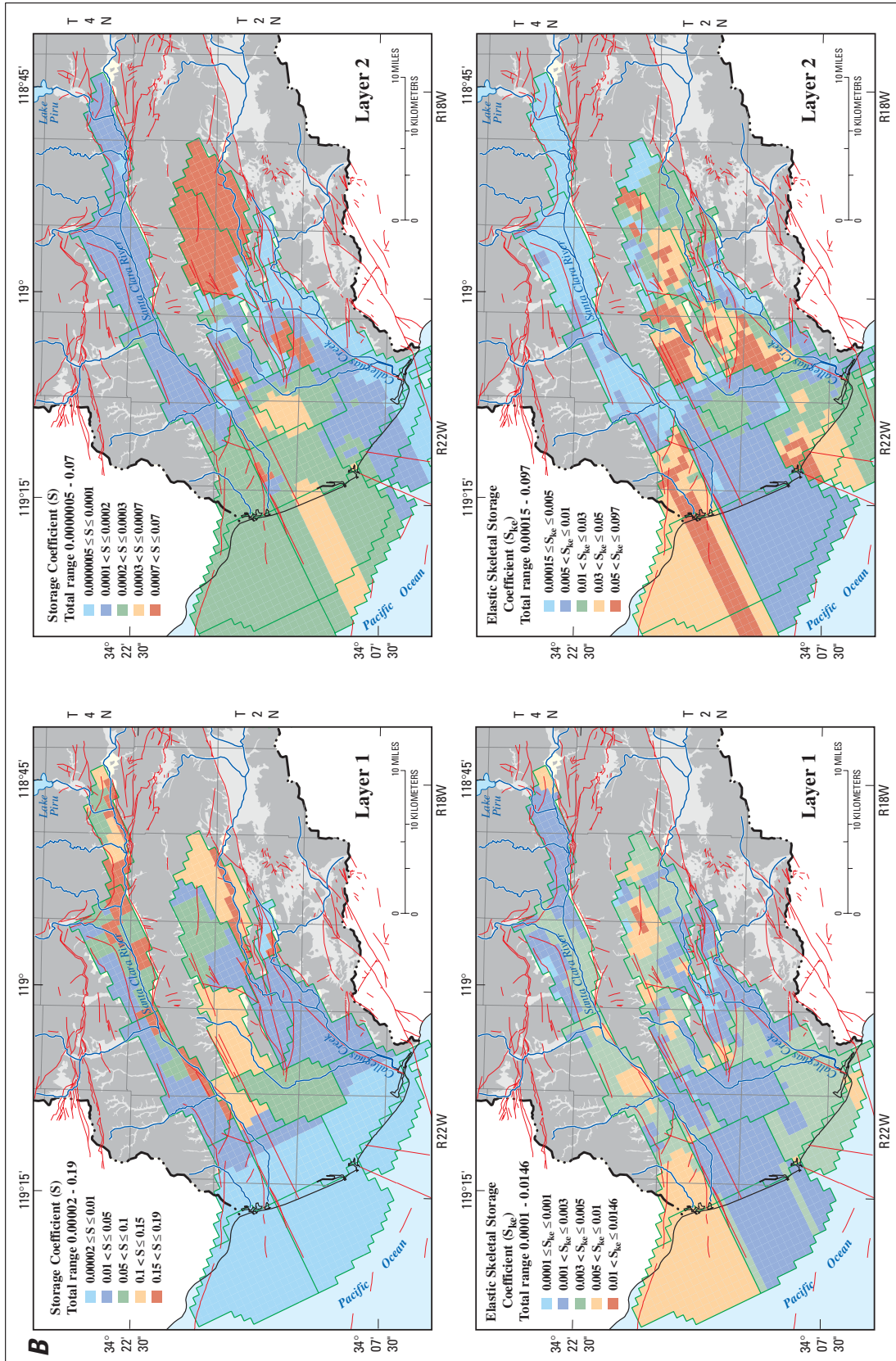


Figure 19—Continued.

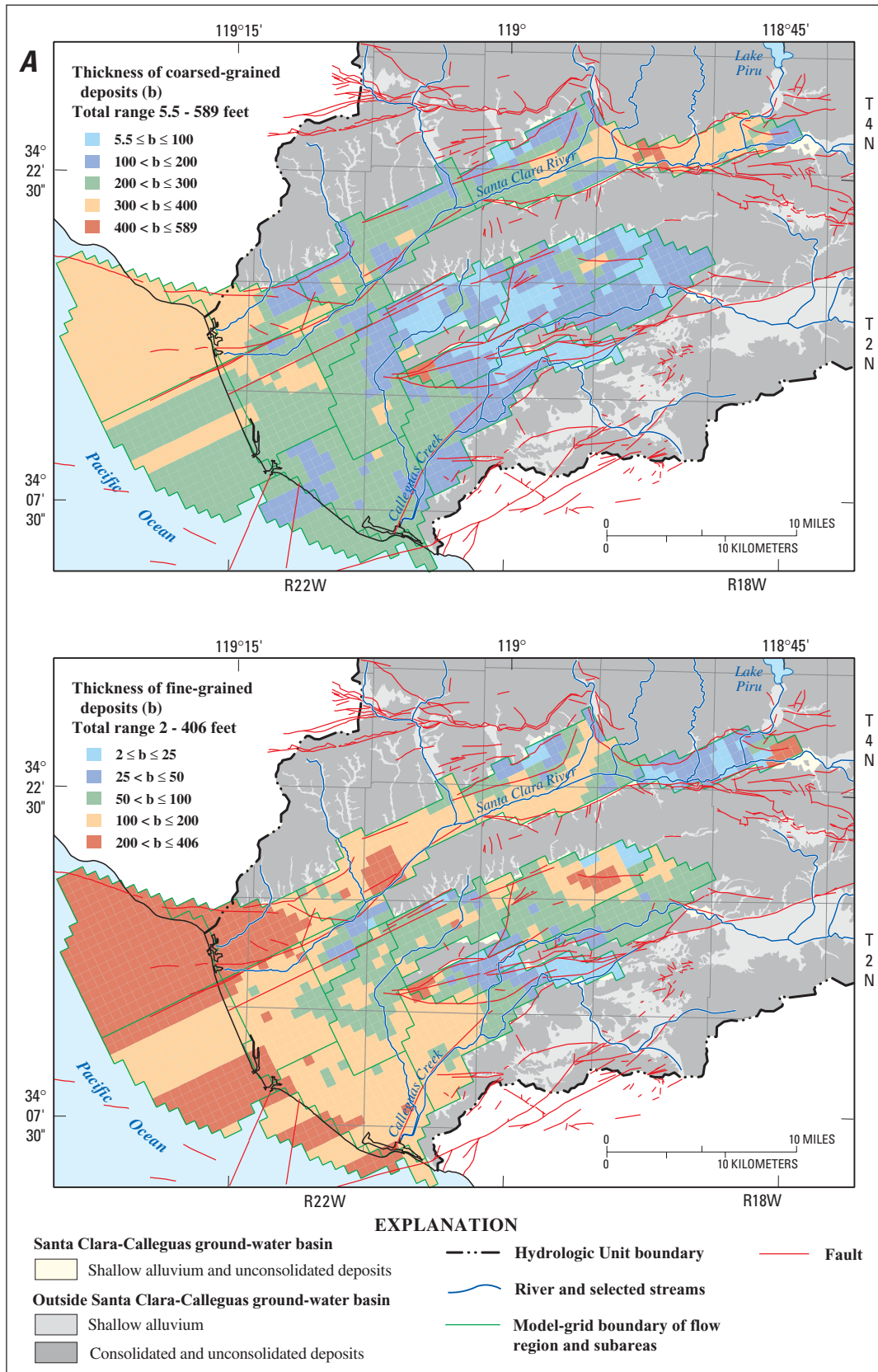


Figure 20. Distribution of estimated total thickness of coarse-grained and fine-grained interbeds used to estimate hydraulic properties and storage properties for the model of the Santa Clara–Calleguas ground-water basin, Ventura County, California. **A**, Upper-aquifer system (model layer 1). **B**, Lower-aquifer system model (layer 2).

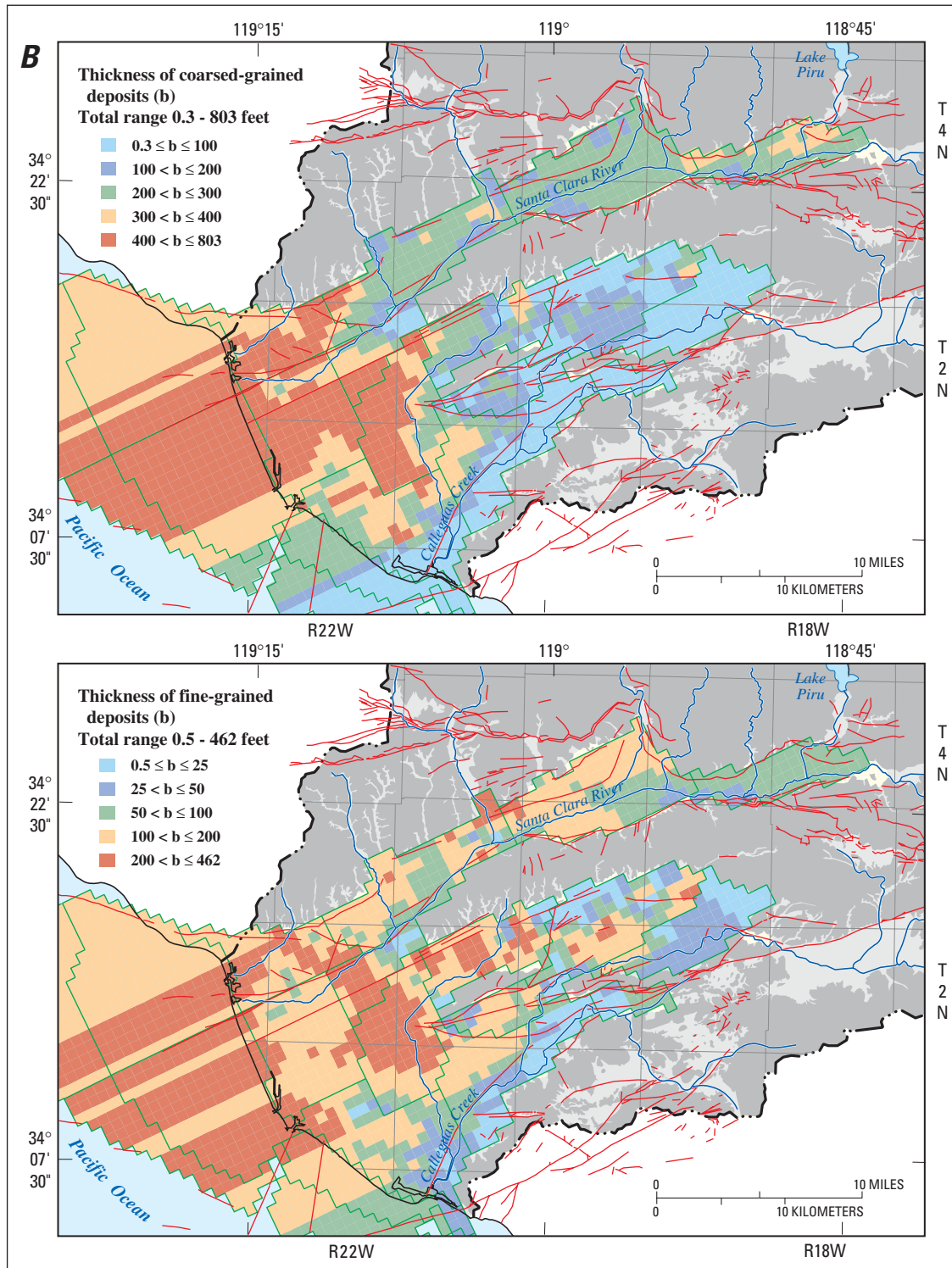


Figure 20—Continued.

Storage Properties

The hydraulic properties used to simulate the changes in storage of water within the aquifer systems consist of three components (Hanson, 1989). The first two components are specific yield and the elastic storage coefficient of the aquifer system, and the third component is the inelastic storage coefficient, which governs the irreversible release of water from the inelastic compaction of the fine-grained deposits. The specific yield and the elastic storage coefficients represent and govern the reversible release and uptake of water from storage. The elastic and inelastic storage coefficient represents the sum of storage owing to the compressibility of water and to the compressibility of the matrix or the skeleton of the aquifer system.

Storage owing to the compressibility of water was estimated as the product of the compressibility and the specific weight of water, the porosity, and the total thicknesses of the coarse- and fine-grained deposits in the aquifer (fig. 20). The assumed porosities were 35 and 25 percent for fine- and coarse-grained deposits, respectively; they were estimated from transport modeling of seawater intrusion along the Hueneme submarine canyon (Tracy Nishikawa, U.S. Geological Survey, written commun., 1994) and range from 1.8×10^{-5} to 2.5×10^{-4} for the upper-aquifer system (layer 1) and from less than 1×10^{-6} to 4.5×10^{-4} for the lower-aquifer system (layer 2). The ranges were specified within MODFLOW as the aquifer-system storage coefficients.

The upper-aquifer system (layer 1) was simulated as unconfined in the Santa Clara Valley, the Las Posas Valley, parts of the Santa Rosa Valley subareas, the Oxnard Plain Forebay subarea, and the Northeast Oxnard Plain subareas (fig. 19B). In the remainder of the Oxnard Plain and the Mound subareas, the upper-aquifer system was simulated as confined. Storage coefficients, estimated from specific yields from previous models, range from 0.01 to 0.19 in the Santa Clara River subareas; the estimate was 0.12 along Conejo Creek in the Santa Rosa Valley subarea. The storage coefficients (specific yields) were assumed to range from 0.02 to 0.19 in the Las Posas Valley subareas (fig. 19B).

The elastic and inelastic skeletal storage coefficients were simulated using the interbed storage package (Leake and Prudic, 1991). The elastic skeletal

storage coefficient of the coarse-grained deposits was estimated from the difference between an estimated aquifer specific storage and the specific storage representing the compressibility of water (Hanson, 1989). Specific storage is the ratio of the storage coefficient to the thickness of the sediments, in this case the aggregate thickness of the coarse-grained deposits. Reported values for aquifer specific storage determined from local aquifer tests in the upper- and lower-aquifer systems range from 1.2×10^{-6} to $2 \times 10^{-6} \text{ ft}^{-1}$ (Neuman and Witherspoon, 1972; Hanson and Nishikawa, 1996). An initial elastic specific storage of $3 \times 10^{-6} \text{ ft}^{-1}$ was assumed from other reported values for alluvial sediments (Ireland and others, 1984; Hanson, 1989). The aquifer elastic skeletal storage coefficient was estimated as the product of the aquifer skeletal specific storage and the aggregate cell-by-cell thickness of the coarse-grained deposits for each model layer (fig. 20). In a similar manner, the elastic skeletal storage coefficient of the fine-grained deposits was estimated from the difference between a specific storage for the fine-grained deposits and the specific storage representing the compressibility of water (Hanson, 1989). The elastic storage coefficient for the fine-grained deposits was estimated as the product of the elastic skeletal specific storage of the fine-grained deposits and the aggregate cell-by-cell thickness of fine-grained deposits for each model layer (fig. 20). The composite aquifer-system elastic skeletal storage coefficient was the sum of the elastic skeletal storage coefficients for the coarse-grained and fine-grained deposits for each cell in each model layer (fig. 19B).

The third component of storage, owing to the inelastic compaction of the fine-grained deposits, was estimated as the product of the inelastic specific storage and the aggregate cell-by-cell thickness of the fine-grained deposits for each model layer (fig. 20). An initial inelastic skeletal specific storage of $2 \times 10^{-4} \text{ ft}^{-1}$ was based on the estimates from a consolidation test performed on the cores of fine-grained deposits from the Oxnard and Mugu aquifers (California Department of Water Resources, 1971, figs. VI-12 and VI-13) and aquifer-test analyses (Neuman and Witherspoon, 1972; Neuman and Gardner, 1989); these estimated range from 1.3×10^{-4} to $4.3 \times 10^{-4} \text{ ft}^{-1}$.

The transition from elastic to inelastic storage is controlled by the preconsolidation stress—the maximum previous load that has been put on each sedimentary layer. The preconsolidation-stress threshold, expressed in terms of equivalent hydraulic head, can range from 50 ft of water-level decline in some well-sorted, fine-grained deposits that have had minimal sedimentary loading or lithification to more than 150 ft of water-level decline in some lithified, compressed, poorly sorted, or coarse-grained deposits (Holzer, 1981). The transition from elastic to inelastic storage was estimated to be 150 ft of water-level decline from predevelopment conditions throughout the lower-aquifer system and 100 ft of water-level decline throughout the upper-aquifer system, with the exception of 50 ft of water-level decline in the upper-aquifer system in the South Oxnard Plain subarea. These estimates were based, in part, on consolidation tests (California Department of Water Resources, 1971), water-level hydrographs ([figs. 13 and 14](#)), subsidence trajectories ([fig. 9C](#)), and lithologic data (Densmore, 1996).

Vertical Leakage

Vertical leakage controls vertical flow between the upper- and lower-aquifer systems. Vertical leakage was calculated for this model ([fig. 19A](#)) as the estimated vertical hydraulic conductivity divided by the combined half-thicknesses of each adjacent model layer for the estimated fine-grained deposits ([fig. 20](#)) in the upper- and lower-aquifer systems (McDonald and Harbaugh, 1988, eq. 5). Estimates of vertical leakage of flow between the upper and lower aquifers used in previous regional models range from less than 9×10^{-6} to 0.002 (ft/d)/ft for the Oxnard Plain subarea (California Department of Water Resources, 1975; Reichard, 1995, [fig. 12](#)). A subregional model developed for the Santa Rosa Valley subarea (Johnson and Yoon, 1987) yielded estimates that range from 1.5×10^{-3} (ft/d)/ft between the alluvium and the underlying Santa Margarita Formation to 3×10^{-5} (ft/d)/ft between the Santa Margarita and Saugus Formations and the underlying Conejo Volcanics. A subregional model developed for Las Posas Valley (CH2M HILL, 1993) used a uniform value of vertical

hydraulic conductivity of 0.05 ft/d to simulate flow across the aquitards separating the Fox Canyon and Grimes Canyon aquifers in the Las Posas Valley subareas. Published values of vertical hydraulic conductivity range from 0.01 to 1×10^{-4} ft/d for the Oxnard Plain subarea (California Department of Water Resources, 1975; Neuman and Gardner, 1989) and from 24. to 6×10^{-4} ft/d for the Pleasant Valley subarea (Hanson and Nishikawa, 1996).

The initial estimates of vertical leakage were from previous ground-water flow models. For the extensions of the two model layers, the initial values used were 1×10^{-6} (ft/d)/ft for the Mound, the Santa Clara River Valley, the Pleasant Valley, and the Santa Rosa Valley subareas and for the offshore regions, and 1×10^{-5} (ft/d)/ft for the Las Posas Valley subareas. These are largely assumed values. The final distribution of vertical leakage was based on fitting simulated head differences to those measured at multiple-well completion sites ([fig. 15](#)). All vertical leakage values were held constant for the period of simulation.

Model Calibration

Calibration of the transient-state simulations was done for 1891–1993 and was based on matching water levels ([fig. 13, 14, 15, and 21](#)) and streamflows ([fig. 22](#)). Predevelopment conditions (steady-state) were used as the initial conditions for the transient-state calibration. The long period of transient simulation was required because features of development, such as coastal landward flow (seawater intrusion) and subsidence, are dependent on the initial state of the aquifer systems.

Calibration Summary

Calibration was achieved through trial-and-error adjustments to recharge, hydraulic properties, and pumpage to achieve a good fit within each subarea over the historical period of record. These adjustments were made as systematically as possible, starting with recharge and streamflow, then hydraulic properties, and finally indirect agricultural pumpage estimates. Calibration and model development began using the extended model developed by Reichard (1995).

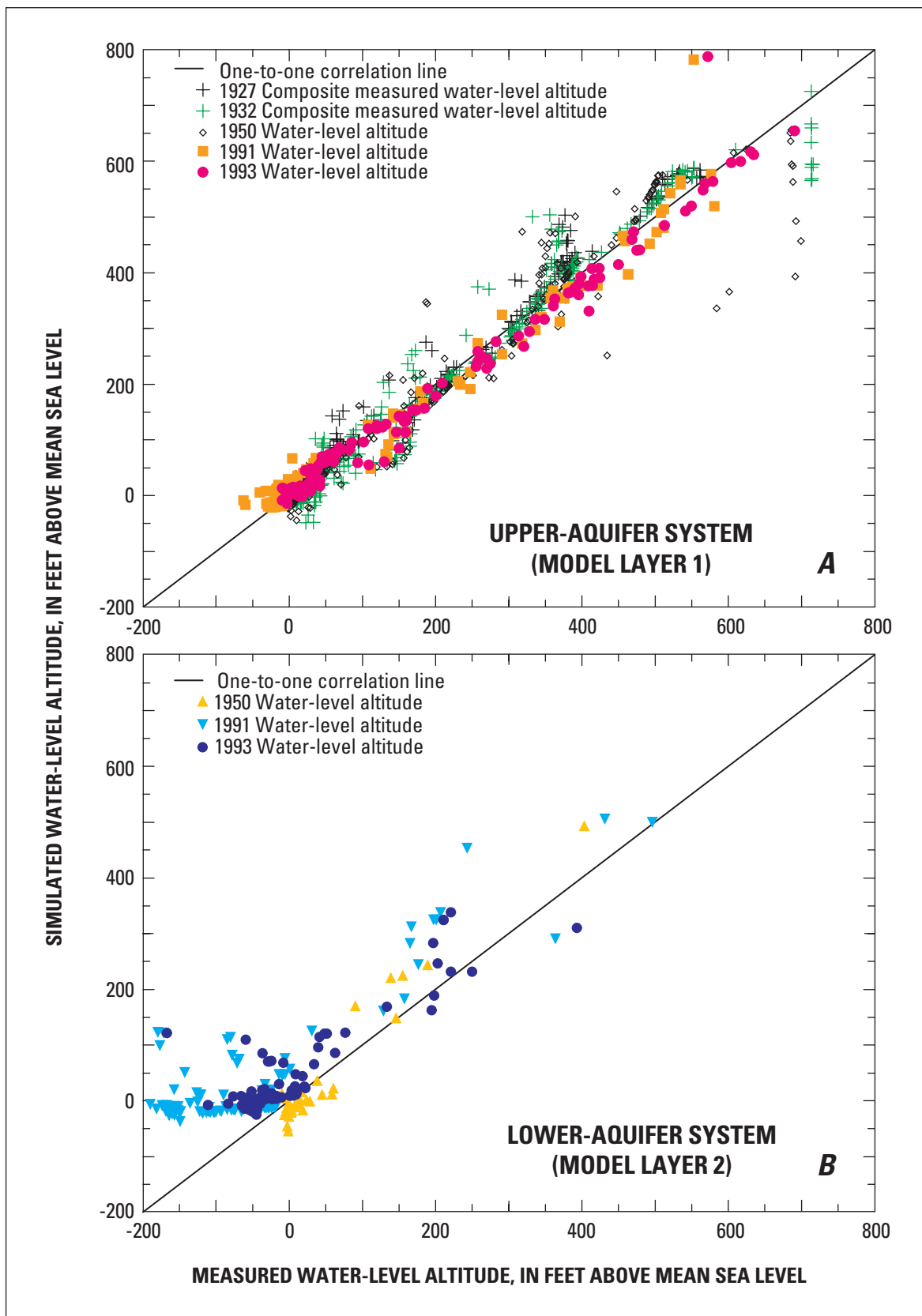


Figure 21. Relation between measured and simulated water-level altitudes for selected years for the transient simulation of developed conditions (1927, 1932, 1950, 1991, and 1993) in the Santa Clara–Calleguas ground-water basin, Ventura County, California. **A**, Upper-aquifer system (model layer 1). **B**, Lower-aquifer system (model layer 2). **C**, Oxnard Plain.

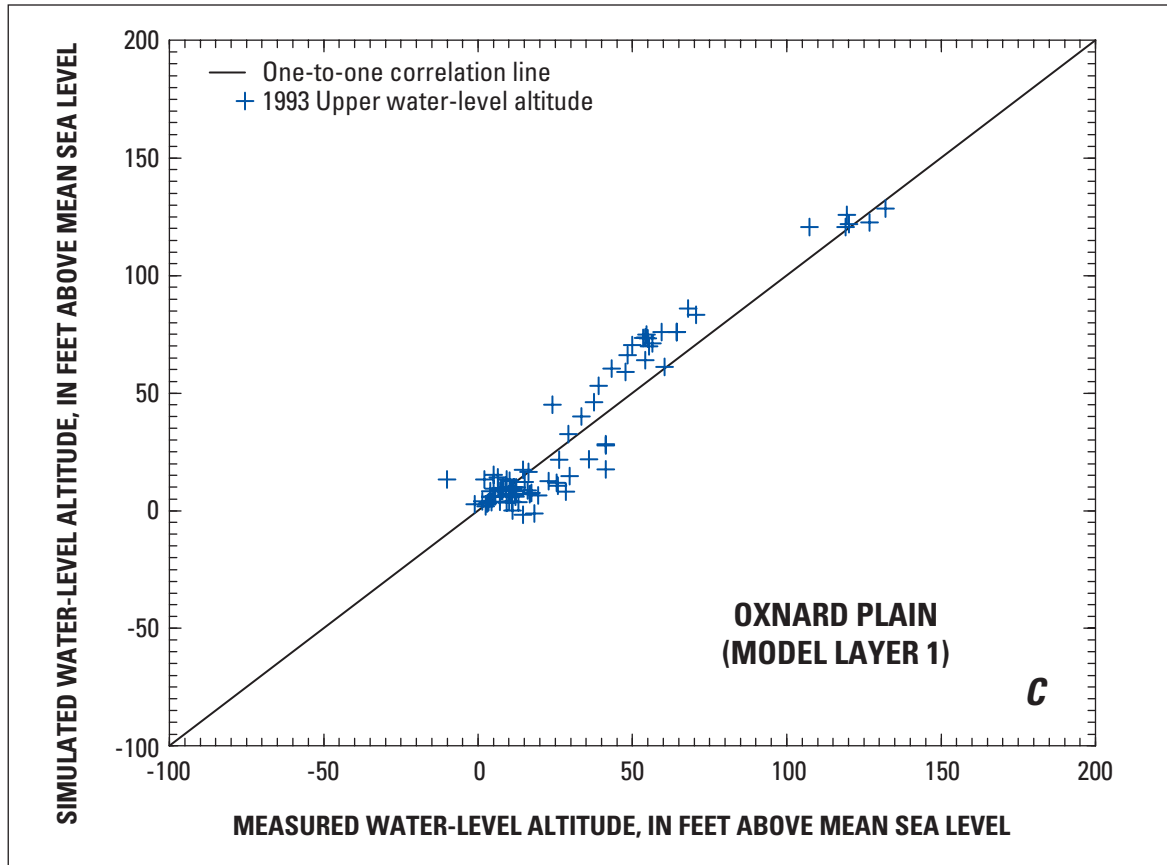


Figure 21—Continued.

Predevelopment Initial Conditions

Calibrating the model was an iterative process between the steady-state and transient-state simulations. The steady-state simulation provided initial conditions for the transient-state calibration. After each transient-state calibration, the updated model parameters were used to simulate updated steady-state conditions prior to additional calibration. The steady-state conditions were dependent on recharge (streamflow, mountain-front recharge, and valley-floor recharge) and discharge (streamflow and ET) from the aquifer system, transmissivity, vertical leakance between layers, fault hydraulic characteristic, and general-head boundary conductance. Because water levels are constant under steady-state conditions,

storage is not required to simulate steady-state conditions. Initial recharge was based on the long-term seasonal geometric-mean ratios of runoff to wet-period winter precipitation. Streamflows were simulated as median streamflows. The composite ET rates and the model cells with the potential for ET for the years 1912, 1927, 1932, and 1950 (Conejo Creek area) were used for the predevelopment simulation (fig. 23). The initial hydraulic properties were based on Reichard's (1995) values and were adjusted during transient-state calibration. Few data were available for comparison of steady-state conditions. However, the simulated initial conditions are considered adequate if water levels are 40 to 50 ft above sea level near the coast along the Oxnard Plain subareas. This requirement was based on a report of early hydraulic conditions (Freeman, 1968).

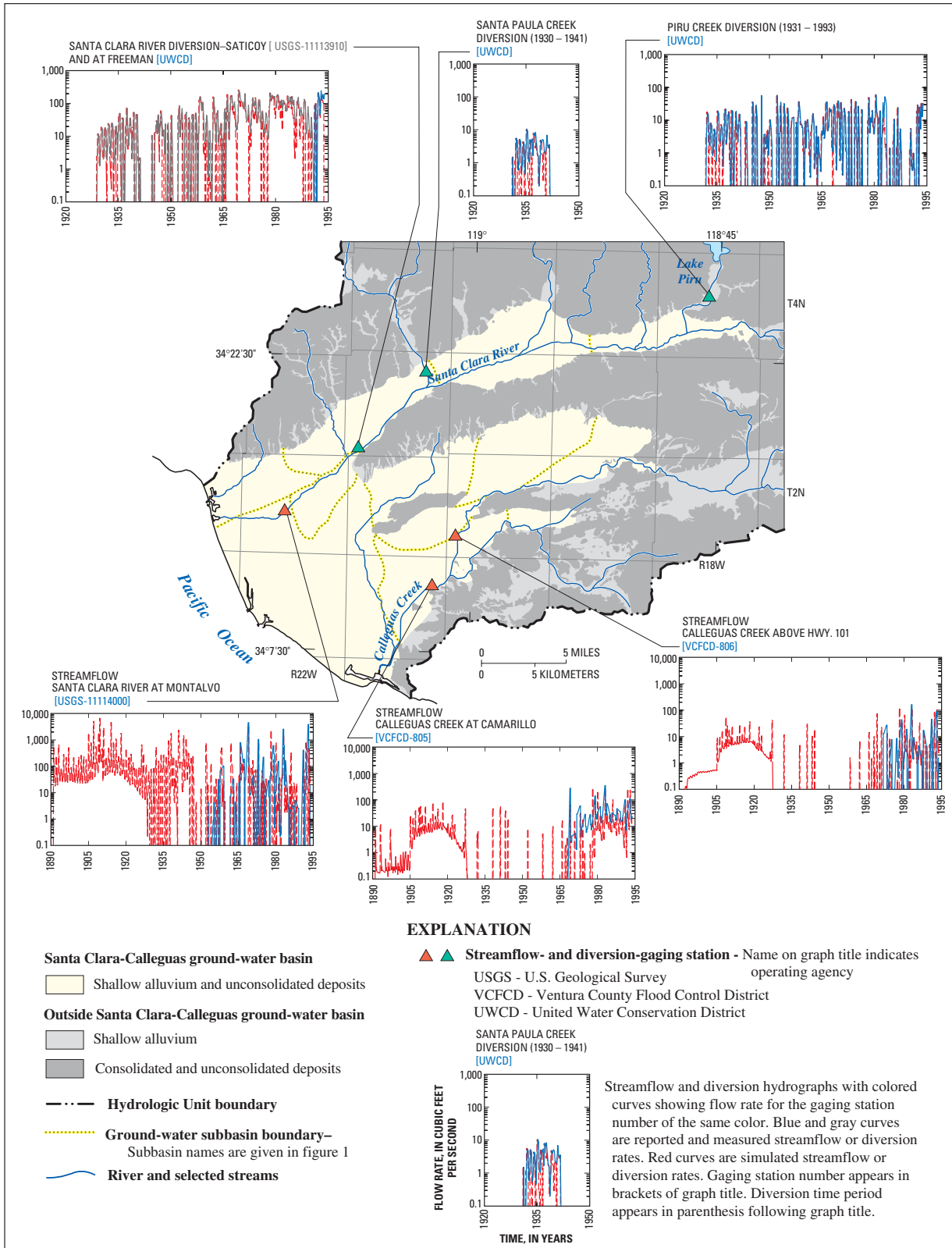


Figure 22. Measured and simulated seasonal streamflows or diversion rates for the Santa Clara–Calleguas ground-water basin, Ventura County, California.

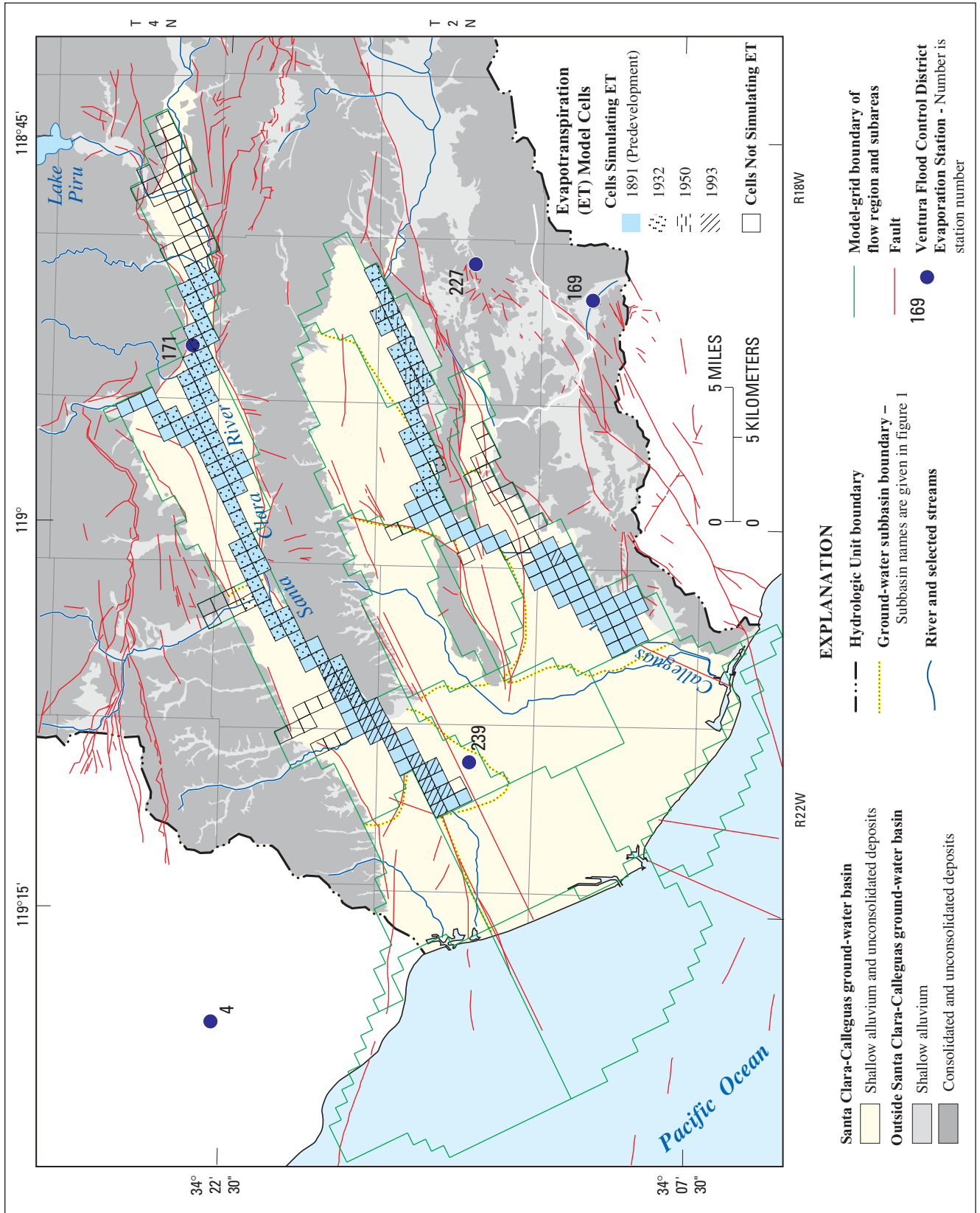


Figure 23. Model cells with simulated evapotranspiration in 1891 (predevelopment), 1932, 1950, and 1993 in the upper layer of the model of the Santa Clara-Calleguas ground-water basin, Ventura County, California.

Transient-State Calibration Parameters

Transient-state conditions were dependent on recharge (streamflow, mountain-front recharge, valley-floor recharge, and artificial recharge) to and discharge (pumpage, streamflow, and ET) from the aquifer system and on transmissivity, storage, vertical leakage between layers, fault hydraulic characteristics, and general-head boundary conductance. Because of the large head differences within some parts of the aquifer systems, water-level maps were used for comparisons but are considered less reliable than time-series data. Estimates of spatial fit were made for selected times of the transient simulation (fig. 21). Calibration was primarily based on temporal comparisons, instead of spatial comparisons, using long-term water-level hydrographs (figs. 13, 14, and 15), streamflow hydrographs (fig. 22) and time-series of bench-mark land-surface altitudes (subsidence trajectories) (fig. 9).

Recharge was adjusted to reduce the overestimation of mountain-front recharge, valley-floor infiltration, and streamflow infiltration. The modified rational method of estimating infiltration tended to overestimate the water available during the wettest seasons; therefore, the upper limit of runoff available for mountain-front recharge was limited to less than 90 percent of average precipitation.

Simulated streamflow infiltration initially was too large when floodflows or intermittent flows were spread over an entire season, and it did not reflect the observed and measured changes in streamflow during low-flow and high-flow conditions. The flow-dependent changes in streambed conductance are believed to be related mostly to changes in channel width. Grouping and varying streambed conductance with flow were critical for accurately depicting water-level declines and recoveries in wells during wet and dry periods (figs. 13 and 14). Grouping and varying streambed conductance for the dry periods helped to simulate a more accurate depiction of the conveyance (delivery) of controlled releases from Lake Piru that are routed down the Santa Clara River and are simulated as

the total reported diversions at Piru, Santa Paula, Saticoy, and Freeman (fig. 22). Segments of the streamflow network in the coastal plain (segments 22, 23, 29, and part of 30) (fig. 18B) are not in direct connection with the upper-aquifer system and therefore were assigned a streambed conductance of zero. This allowed the simulated water levels for predevelopment conditions and the recovery periods for development conditions to rebound to the measured water levels (figs. 13 and 14). Streamflow was increased from about 1.5 to 14 ft³/s for Arroyo Simi to account for treated-sewage effluent discharged between 1964 and 1993. On the basis of streamflow data from the hydrographs for Calleguas Creek at Camarillo (fig. 22, VCFC station 805), the initial discharge (1964–79) was estimated to start at 1.5 ft³/s and increase linearly to 10 ft³/s.

The hydraulic properties estimated by Reichard (1995) were adjusted during model calibration; they include transmissivity, storage properties, and vertical leakage. The initial estimates were described earlier (see section on “Hydraulic Properties”). The only change to the storage properties was the transformation of Reichard’s (1995) initial estimates to cell-by-cell estimates, as was described earlier. Additional calibration also was done for fault hydraulic characteristics and offshore general-head boundary conductance. These properties were adjusted for the period of reported pumpage largely on the basis of the water levels in the hydrographs.

Transmissivity values were reduced by a factor of 0.55 for the lower layer of the Port Hueneme area and were increased by a factor of 1.5 for the lower layer of the East Las Posas Valley subarea (figs. 17B and 19A) compared with the values used by Reichard (1995). The decrease in transmissivities in the lower layer brought the values closer to those in the transport model of the Port Hueneme area (Nishikawa, 1997) and to those estimated from aquifer tests completed in the East Las Posas Valley area (CH2M HILL, 1992). The transmissivities of the aquifer layer underlying the major streams and tributaries also were increased during model calibration.

Adjustments in vertical leakance were made on the basis of water-level differences at multiple-well observation sites and, for some areas, on the basis of data from the hydrographs of selected production wells. Recall that the vertical leakances were calculated as the estimated vertical hydraulic conductivity divided by the combined half-thicknesses of the estimated fine-grained deposits in the upper- and lower-aquifer systems (McDonald and Harbaugh, 1988, eq. 51). Cell-by-cell estimates for the West Las Posas Valley subarea were based on a vertical hydraulic conductivity of 0.0005 ft/d. Cell-by-cell estimates for the Forebay region of the Oxnard Plain were based on a vertical hydraulic conductivity of 0.001 ft/d for all but five cells in the Saticoy area, for which a value of 0.01 ft/d was used. The final distribution of vertical leakances ranged from 1×10^{-7} to 3.03×10^{-5} (ft/d)/ft (fig. 19A). Cell-by-cell estimates initially were made for all the subareas, but the estimates did not improve model fit for the East and South Las Posas Valley subareas. For these two subareas, estimates were not based on the thickness of the fine-grained deposits; the final calibrated vertical leakances align with the underlying syncline-anticline structures within the lower-aquifer system (figs. 9 and 20).

Although pumpage was the largest stress in the model, some uncertainty remained about the accuracy of the land-use estimates of pumpage. Some adjustments in the magnitude and distribution of the pumpage estimated from land use were made during the calibration of the flow model in order to have the model enter the final 10-years of reported pumpage at the correct water-level altitudes. These changes were largely based on the measured temporal variations in

ground-water levels in the subareas and on the magnitude and changes of pumpage for the 1983–93 period of reported pumpage. Changes to land-use estimates of historical pumpage include elimination of pumpage from the Santa Clara River Valley subareas and the Oxnard Plain Forebay subarea for 1891–1918 so that the first significant ground-water pumpage began with the dry period of 1919–36. The 1950 and 1969 estimates of the land-use-based pumpage also had to be modified for selected subareas. The changes in the 1950 estimate of agricultural pumpage applied over the period 1946–61 ranged from a 34-percent reduction in pumpage for the Mound subbasin to an approximate 300-percent increase for the Piru subbasin; the changes in the 1969 estimate applied over the period 1962–77 ranged from a 34-percent reduction for the Mound subarea to an approximate 100-percent increase in the North and South Pleasant Valley and the Piru subareas. These changes brought the estimated historical agricultural pumpage into alignment with the reported agricultural pumpage (fig. 11B) and improved the alignment between the measured and simulated ground-water levels and the land-use changes in various subareas for these two periods. Pumpage was reduced to 40 percent of the 1932 estimate for the years 1935–45, which span the post-Great Depression and World War II period, as well as a severe drought that was followed by one of the wettest periods on record (fig. 2). This reduction was the only way to achieve the record water-level recoveries that have been equaled only during predevelopment conditions and more recently during 1993. These adjustments did not affect calibration of hydraulic properties or recharge during the period of reported pumpage.

The percentage of pumpage between layers was changed during model calibration. The final vertical distribution of pumpage between the model layers for wells spanning both model layers is summarized in [figure 7B](#) for all the subareas.

The general-head boundaries that initially were placed at the submarine outcrops were moved landward to better represent the average location of the freshwater-saltwater interface. The values of the boundary heads were aligned with the top of the basal coarse-grained layers in the Oxnard and Hueneme aquifers for the upper- and lower-aquifer systems, respectively. The boundary conductances were grouped into several coastal subreaches with different values, grouping the conductances, however, did not improve model fit. The final configuration consisted of a single value for each model layer, which was the simplest approach without additional data and was adequate for matching water levels along the coast. The flows at the general-head boundaries were monitored to verify that simulated outflow was occurring during wet periods when recovery of water levels exceeded the specified heads of the seawater at the general-head boundary. To be consistent, the model should simulate coastal landward flow (seawater intrusion) during the major droughts when water levels decline below the heads of the denser seawater. The current model is consistent with the concept of the wet-period outflow, as shown by the outflows of 1984–93 ([figure 25B](#) in the section “Transient-State Model Comparisons”), and with the concept of coastal landward flow (seawater intrusion) during droughts, such as the drought of 1987–91.

Transient-State Model Comparisons

Calibration and goodness-of-fit of the transient-state model were determined by comparing simulated values with measured values for ground-water levels, streamflow, and land subsidence. The simulated water levels were compared with water-level maps for 1932 and 1993 ([fig. 12](#)) and correlated with the water-level data for 1927, 1932, 1950, 1991, and 1993 ([fig. 21](#)) and the water-level hydrographs of selected production wells ([figs. 13 and 14](#)) and multiple-well observation sites ([fig. 15](#)). A comparison of simulated streamflow was made for the downstream gaging stations and the streamflow-diversion sites ([fig. 22](#)). The spatial

distribution of potential ET, based on riparian vegetation, and the spatial distribution of simulated ET for predevelopment and developed conditions in 1932, 1950, and 1993 were also compared ([fig. 23](#)). Measured and simulated subsidence for selected bench marks ([fig. 24](#)) were used to compare the potential effects of water-level declines on simulated subsidence in the South Oxnard Plain subarea. And, finally, selected comparisons of ground-water flows were used to confirm that flows within the model ([fig. 25](#)) were conceptually consistent with the framework provided by geohydrologic and geochemical analyses.

The best and primary comparison period is the 10-year period of reported pumpage, 1984–93, which represents one dry period and parts of two wet periods ([fig. 2A](#)). Within this period is a 4-year period (1990–93) for which measured water levels and water-level differences between aquifer systems measured at the multiple-well monitoring sites ([fig. 15](#)) can be compared with model results.

The model generally matched the measured water-level, streamflow, and bench-mark data for the calibration period ([figs. 12, 13–15, 21; 22, and 24](#), respectively). Comparisons of the simulated and measured water levels estimated from land-use maps have some uncertainty because the measured ground-water levels reflect a wide variety of screened intervals in wells, and the “synoptic” measured water levels reflect water levels measured over spans of several months over a season ([fig. 12A,B](#)). The model slightly overestimates historical water-level altitudes for the early period of development ([fig. 12A](#)). The correlation diagram on [figure 12A](#) shows no systematic discrepancies between measured and simulated water levels in the upper-aquifer system. Measured minus simulated water levels have a mean error (ME) for the upper aquifer system of –22.8 ft and a root mean square error (RMSE) of 35.2 ft for 1927 (number of comparison wells: N = 169), and a ME of 7.29 ft and a RMSE of 42.2 ft for 1932 (N = 354). A comparison of the measured and simulated water levels for 1932 ([fig. 12A](#)) indicate similar patterns. Water-level differences between simulated and measured data range from less than 5 ft near the coast to about 40 ft in the Forebay, and they are less than 20 to 40 ft in the Santa Clara River Valley and Pleasant Valley subareas.

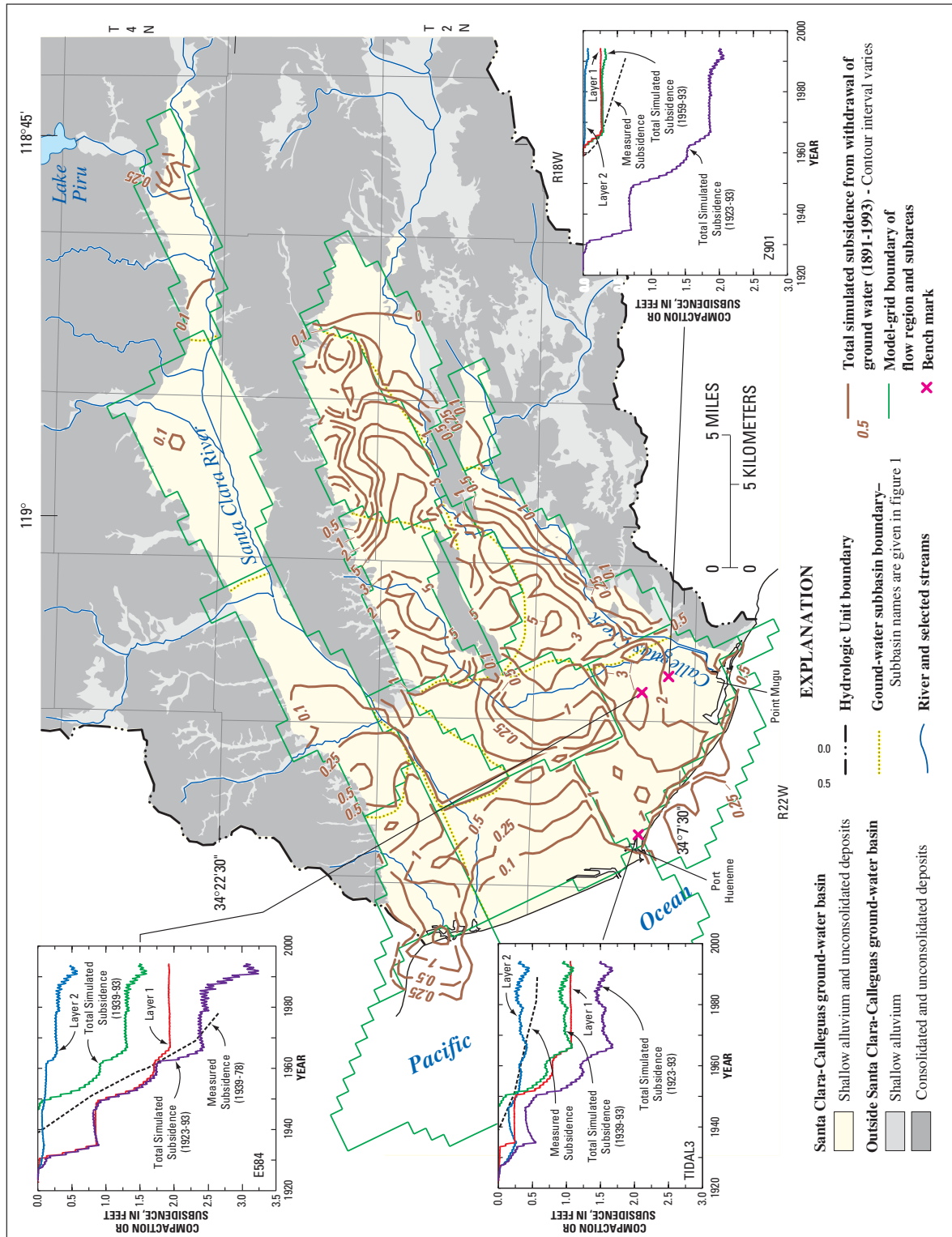


Figure 24. Simulated compaction owing to withdrawal of ground water, 1891–1993, in the Santa Clara–Calleguas ground-water basin, Ventura County, California, and locations of selected bench marks and related measured and simulated bench-mark trajectories.

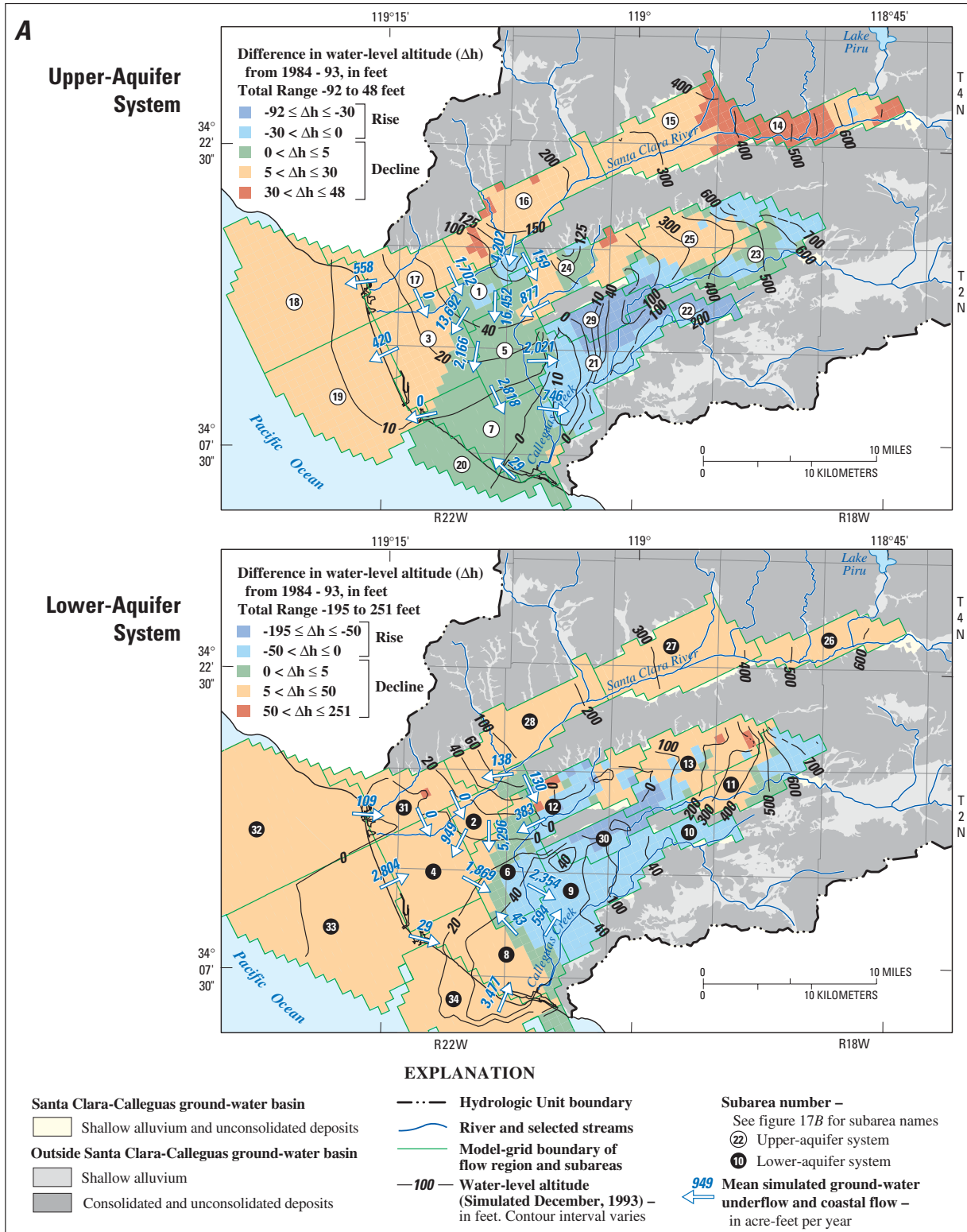
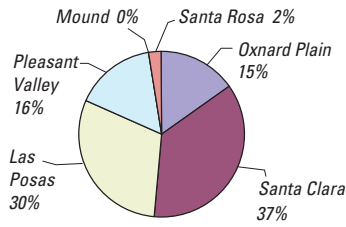


Figure 25. A, Simulated water-altitudes (December 1992), decline in ground-water levels from 1984 to 1994, and mean ground-water flow in the Santa Clara-Calleguas ground-water basin, Ventura County, California. B, Cumulative changes in ground-water storage and ground-water flow for selected subareas during 1984-93. C, Hydrologic budgets for predevelopment conditions. D, Hydrologic budgets for 1984-93 period.

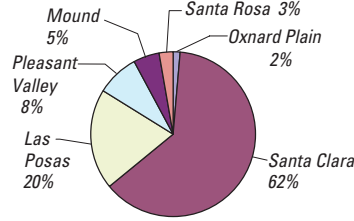
C

Predevelopment Conditions

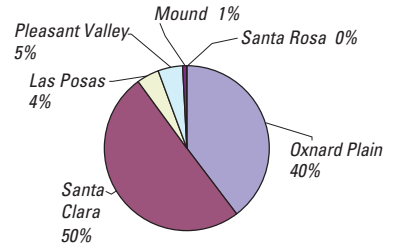
Valley-Floor Recharge
4,770 acre-feet per year



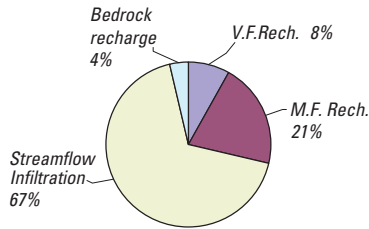
Mountain-Front and Bedrock Recharge
14,600 acre-feet per year



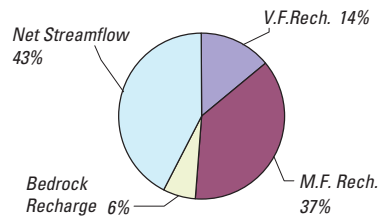
Net Streamflow Recharge
14,300 acre-feet per year



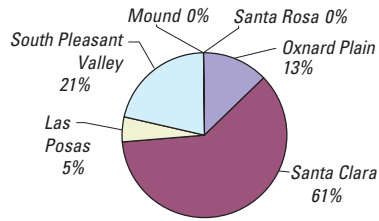
Total Recharge
59,900 acre-feet per year



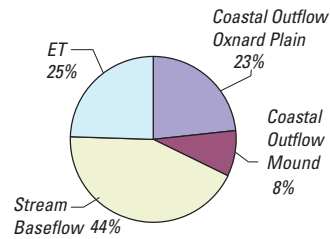
Total Net Recharge
33,650 acre-feet per year



Evapotranspiration
14,800 acre-feet per year



Total Discharge
59,900 acre-feet per year



ET = Evapotranspiration
V.F. Rech. = Valley-Floor Recharge
M.F. Rech. = Mountain-Front and Bedrock Recharge

Figure 25—Continued.

D

Historical Period 1984-93

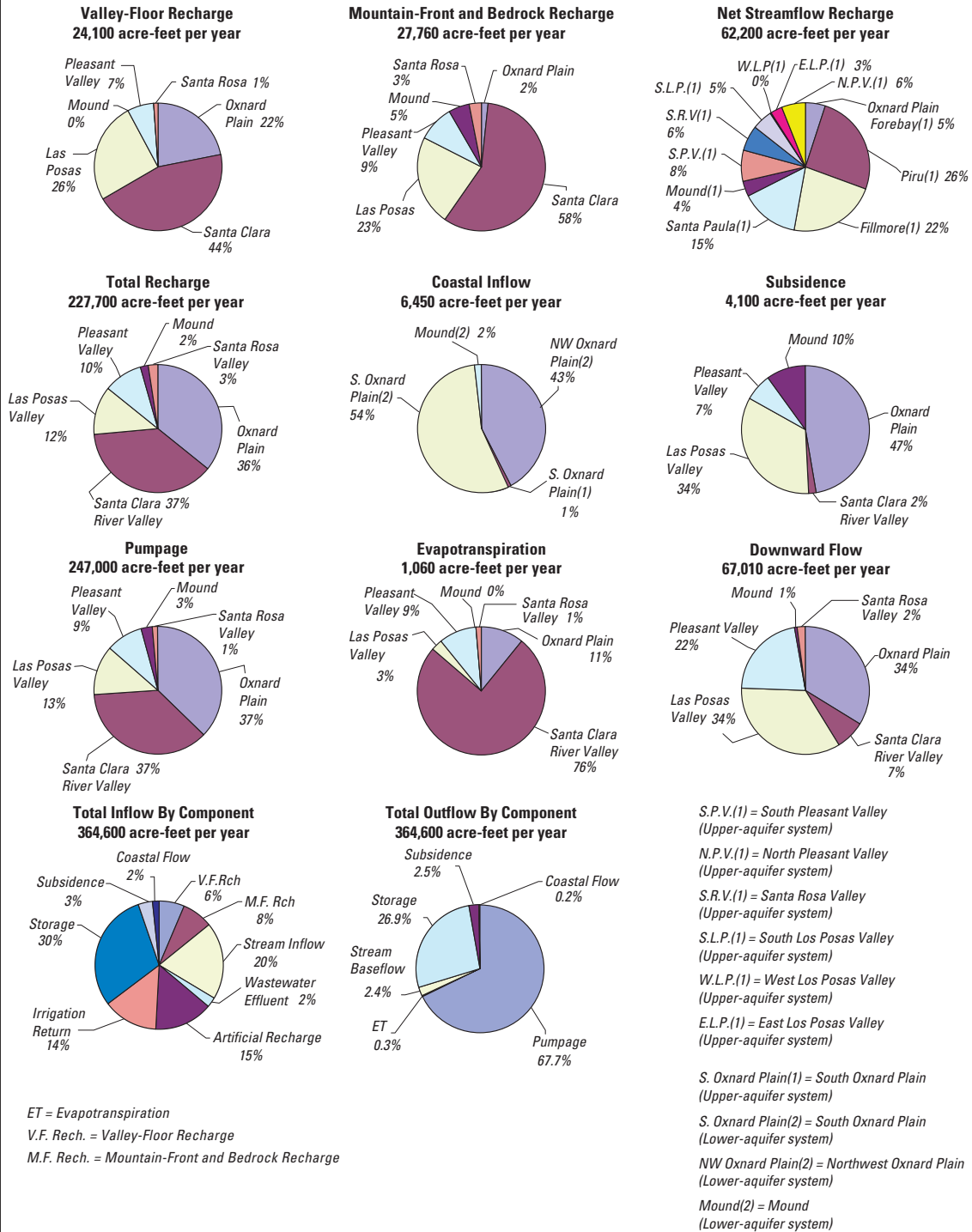


Figure 25—Continued.

The simulated water levels were lower than the measured water levels for 1950, the first period of substantial ground-water development in both aquifer systems [ME and RMSE are 9.95 and 52.7 ft, respectively, for the upper-aquifer system (N = 297) (fig. 21A), and 8.39 and 39.3 ft, respectively, for the lower-aquifer system (N = 31) (fig. 21B)]. The simulated water levels for the 1987–91 drought were lower than the measured water levels in the upper-aquifer system [ME and RMSE are 1.96 ft and 26.1 ft, respectively, (N = 130) (fig. 21A)] and higher than the measured water levels in the lower-aquifer system [ME and RMSE are –89.8 ft and 110.4 ft, respectively (N = 101) (fig. 21B)]. The differences between the measured and simulated water levels in the lower-aquifer system are, in part, due to the many wells used for the calibration which are completed solely in the Fox Canyon or Grimes Canyon aquifer in parts of the Pleasant Valley and Las Posas Valley subareas. These aquifers were not simulated as separate aquifer layers in the current model and therefore the simulation represents the average water level for the entire lower aquifer system. The Fox Canyon and Grimes Canyon aquifers are relatively low-permeability aquifers; pumpage from these aquifers resulted in large water-level declines. The overlying Hueneme aquifer is relatively more permeable; pumpage from this aquifer resulted in smaller water-level declines. Measured water levels for the multiple-well monitoring sites indicate water-level differences within the lower-aquifer system of as much as 75 ft between the Hueneme aquifer and the Fox Canyon and Grimes aquifers (fig. 15). The model was calibrated to the Hueneme aquifer and would have required additional layers to simulate the water-level differences for the lower aquifers. Some water-level measurements also may have been affected by pumping, which resulted in measured water levels being lower than the simulated levels. Another reason for the water-level differences may be that instantaneous water-level measurements were compared with simulated water levels controlled by average seasonal pumpage.

Measured water levels for the 1992–93 wet-period recovered; the simulated water levels were lower than the measured water levels for the upper-aquifer system [ME and RMSE are 9.68 ft and 20.5 ft, respectively (N = 161) (fig. 21A)] and higher than the measured water levels in the lower-aquifer system [ME and RMSE are –42.3 ft and 66.9 ft, respectively (N = 94) (fig. 21B)]. When the comparison was restricted to the upper-aquifer system of the Oxnard Plain for spring 1993, the simulated water levels were only slightly lower than the measured water levels [ME and RMSE are 1.61 ft and 10.7 ft, respectively (N = 90) (fig. 21C)].

In general, the long-term water-level hydrographs (figs. 13 and 14) indicate that the match between measured and simulated water-level altitudes is good for the entire period of simulation, especially those for the Oxnard Plain subbasin. However, some hydrographs show large discrepancies between the simulated and measured water levels; examples of these discrepancies can be seen on the hydrographs of wells along Beardsley Wash, such as well 2N/21W-16J1 in the West Las Posas Valley subarea and wells along the Santa Clara River, wells 2N/22W-2C1 and 3N/22W-36K2 in the Santa Paula subarea, well 2N/22W-9J1 in the Mound subarea, and well 3N/19W-29E2 in the East Las Posas Valley subarea (fig. 14). A comparison of the short-term hydrographs for the RASA multiple-well monitoring sites shows good agreement between the simulated and measured water levels (fig. 15). The simulated water-level differences between the upper and lower layers closely match the measured seasonal and multiple-year patterns of water-level differences (fig. 15). This indicates that the collective estimates of vertical leakance, vertical distribution of pumpage, and recharge are reasonable.

Water-level differences between wells across faults were calibrated by adjusting fault hydraulic characteristics; for example, the water-level differences between well 2N/20W-23K1 (fig. 13) and well 2N/20W-23R1 (fig. 14) across the San Pedro (Bailey) Fault in the Santa Rosa Valley subarea.

Seasonal water-level variations in the upper-aquifer system are controlled largely by streamflow infiltration and related streambed conductance; these factors, when combined with seasonally and climatically variable pumpage, resulted in water-level fluctuations of tens to a hundred feet in wells in the Santa Clara River Valley subareas [wells 4N/19W-25K2, 30R1; 22N/22W-11A1,2 (fig. 14)]. Water-level fluctuations in the Oxnard Plain Forebay subareas include the effects of artificial recharge and pumping back artificially recharged water [wells 2N/22W-12R1, 22R1 (fig. 14); wells 2N/22W-23B3-7, 2N/21W-7L3-6 (fig. 15)].

Simulated streamflows for Montalvo and for the Piru, Santa Paula, Saticoy, and Freeman diversions closely match measured streamflow along the Santa Clara River system. Simulated streamflows also match many of the historical high flow events (figs. 2B and 22); however, they overestimate low streamflow conditions (less than 10 ft³/s) for some dry-year periods at Montalvo on the Santa Clara River (fig. 22). The simulations underestimated the diversions for some dry-year periods when flows were less than 2 to 10 ft³/s at Saticoy and less than 2 ft³/s at the Santa Paula and Piru diversions (fig. 22). Simulated streamflows for Camarillo and above Highway 101 in Calleguas Creek match measured streamflow; the simulated streamflow is intermittent in character after the onset of ground-water development in the late 1920s (fig. 22).

Simulation results indicate that land subsidence started as early as the 1920s and continued through 1984-93, the period when water levels declined below the water levels of the 1950s and 1960s. Results also indicate that preconsolidation may vary considerably and that subsidence occurred primarily during dry-year periods when seasonal and multiple-year water-level declines exceeded past declines in the South Oxnard Plain, Las Posas Valley, and Pleasant Valley subareas (figs. 24 and 25B). Subsidence started in the upper-aquifer system in the South Oxnard Plain subarea during the early period of development (1939-60) (fig. 24). Subsidence has continued, in part, because of the development of the lower-aquifer system, which has contributed most of the subsidence in recent decades (1959-93) (fig. 24).

Simulated subsidence generally matches total measured subsidence in the South Oxnard Plain subarea (fig. 24). The time-series comparisons of subsidence from bench-mark measurements are similar in trend but underestimate subsidence at BM Z 901 near Point Mugu and overestimate subsidence at BM TIDAL 3 near Port Hueneme (fig. 24). The extent of subsidence generally is not well known for areas outside the South Oxnard Plain subarea but may be overestimated for parts of the Pleasant and Las Posas Valley subareas. Field inspections throughout West and East Las Posas subareas did not reveal any surface expressions of land subsidence that would be expected for the amount of simulated subsidence. This overestimation may be caused by overestimation of inelastic skeletal specific storage, overestimation of the aggregate thickness of fine-grained material that is actually subject to loading from water-level declines, and a lack of separate model layers within the lower-aquifer system for the Pleasant and Las Posas Valley subareas. A detailed land survey or Interferometric Synthetic Aperture Radar (InSAR) imagery analysis would be needed to resolve this issue.

Model Uncertainty, Sensitivity, and Limitations

Numerical models of ground-water flow are useful tools for assessing the response of an aquifer system to changing natural and human-induced stresses. Regional-scale models are especially useful for assessing many of the components in the hydrologic cycle and the collective effect of ground-water development in separate subareas of a regional ground-water system. Models, however, are only an approximation of actual systems and typically are based on average and estimated conditions. The reliability or certainty with which a model can simulate aquifer response is directly related to the accuracy of the input data, the amount of detail that can be simulated at the scale of the model, and the model discretization of time and space. Hence, the regional models can be useful for simulating subregional and regional performance of a flow system and for providing boundary information for more detailed local-scale models even though the results of the regional model for a local scale may not be appropriate for site-specific problems such as the performance at a particular well.

The certainty of a model is inversely related to the duration, magnitude, and distribution of simulated inflows and outflows. Thus, better time-varying estimates of pumpage, recharge, irrigation return flow, streamflow, and coastal landward flow (seawater intrusion) could improve simulation of historical development. Additionally, the trial-and-error calibration process is inexact, and this problem is compounded by uncertainty of the variables and by sensitivity of the aquifer-parameter and boundary-condition estimates. Uncertainty in model attributes results in a broader range of possible aquifer-parameter and boundary-condition estimates used to constrain calibration of the ground-water flow model. Uncertainty in water levels in wells, streamflows, and altitudes of bench marks used for model comparison during calibration can affect the degree of fit achieved. Sensitivity to changes in model parameters and boundary conditions during calibration also can affect the degree of fit and the possible range of values used to simulate historical ground-water flow.

An exhaustive analysis of the uncertainty and sensitivity of every model parameter and boundary condition is beyond the purpose and scope of this report. However, a summary can yield insight into the capabilities and limitations of the model, and specific insight into its performance with respect to ground-water management. The combination of the uncertainty in the model-input and comparison data and the sensitivity of the model to changes in model input yield a qualitative measure of the importance of various model attributes. For example, uncertainties in the measurement of streamflows may contribute to uncertainties in the simulation of streamflows and

affect the comparison between measured and simulated streamflows. Based on gaging-station ratings, inaccuracy in streamflow measurements can range from 5 to 20 percent. For high flows, this inaccuracy may result in an uncertainty of hundreds to thousands of acre-feet in potential recharge for some wet years. Other sources of uncertainty include estimates of precipitation, which may have estimation errors (kriging errors) ranging from 5 to 10 percent which can result in thousands of acre-feet of uncertainty for wet-year seasons; estimates of irrigation return flow, which may have estimation errors ranging from 10 to 20 percent owing to the uncertainty and the variability of the estimates of applied water and irrigation efficiency (Koczot, 1996); and errors in the assignment of percentages of pumpage for wells completed across both aquifer systems, which may range from 10 to 20 percent.

Additional uncertainties also may exist with respect to boundary conditions such as the average location of the seawater front, which is represented by the general-head boundary cells; horizontal-flow barriers, some of which may be of inferred extent; and the conductance of some faults. The importance of some faults remains uncertain; for example, faults whose traces generally are parallel to the hydraulic gradient, such as the Oak Ridge and McGrath Faults in the upper-aquifer system, or faults that are adjacent to a spatial contrast in transmissivity, such as the Country Club Fault. Considerable testing of these boundaries was done during model calibration; the resulting estimates for boundary locations and conductance satisfy the conceptual framework and the measured comparison data.